# Revisiting Bloch electrons in a magnetic field: Hofstadter physics via hybrid Wannier states

Xiaoyu Wang [1,*] and Oskar Vafek [1,2,†]
[1]*National High Magnetic Field Lab, Tallahassee, Florida 32310, USA*
[2]*Department of Physics, Florida State University, Tallahassee, Florida 32306, USA*

(Received 6 April 2023; revised 22 September 2023; accepted 14 November 2023; published 4 December 2023)

We revisit the Hofstadter butterfly for a subset of topologically trivial Bloch bands arising from a continuum free electron Hamiltonian in a periodic lattice potential. We employ the recently developed procedure, which was previously used to analyze the case of topologically nontrivial bands [Wang and Vafek, Phys. Rev. B **106**, L121111 (2022)], to construct the finite-field Hilbert space from the zero-field hybrid Wannier basis states. Such states are Bloch extended along one direction and exponentially localized along the other. The method is illustrated for square and triangular lattice potentials and is shown to reproduce all the main features of the Hofstadter spectrum obtained from a numerically exact Landau level expansion method. In the regime where magnetic length is much longer than the spatial extent of the hybrid Wannier state in the localized direction we recover the well-known Harper equation. Because the method applies to both topologically trivial and nontrivial bands, it provides an alternative and efficient approach to moiré materials in magnetic field.

DOI: 10.1103/PhysRevB.108.245109

## I. INTRODUCTION

The discovery of superconductivity and correlated insulating states in twisted bilayer graphene (TBG) [1,2] has invigorated the study of various two-dimensional (2D) moiré electronic materials [3–10]. The moiré superlattice is generated by stacking 2D layered structures either with a small twist or via microscopic lattice mismatch. Despite the large moiré unit cell containing as many as ∼10 000 atoms, the low-energy physics is dominated by only a few isolated narrow Bloch bands formed due to the moiré superlattice potential, motivating theoretical studies that focus on these low-energy degrees of freedom [11–22].

The large moiré unit cell has also enabled the study of magnetic field effects in such systems in the regime with a considerable fraction of one full magnetic flux quantum per moiré unit cell. Electronic interaction effects intermixed with strong magnetic fields have been studied in various moiré materials, revealing not only Landau level degeneracies indicative of the symmetry-breaking phases at zero magnetic field but also novel field-induced insulating states that can carry finite Chern numbers [23–32]. These experimental results in turn motivated further theoretical studies of Hofstadter physics [33–38].

Traditionally, Bloch electrons in magnetic field $\mathbf{B}$ have been studied either by solving the continuum Hamiltonian $\hat{H}(\mathbf{r}, \hat{\mathbf{p}} + \frac{e}{c}\mathbf{A})$, where the magnetic vector potential satisfies $\mathbf{B} = \nabla \times \mathbf{A}$, or via Peierls phase substitution of hopping amplitudes [39–42]. The latter is justified if the subset of Bloch bands of interest at zero field is amenable to a tight-binding description, i.e., there is no topological obstruction to Wannierization. In the first approach, one calculates the matrix elements of $\hat{H}$, including the periodic lattice potential, in the Hilbert space spanned by Landau level (LL) wave functions (obtained without the periodic lattice potential) and diagonalizes the resulting matrix. To achieve numerical convergence within an energy window $W$ an upper LL index cutoff $N_c \sim \lambda W/\hbar\omega_c$ is needed, where $\omega_c = eB/m_e c$ is the cyclotron frequency, $m_e$ is the bare electron mass, and $\lambda$ is a number that increases with the strength of the periodic lattice potential $V$. For example, Ref. [33] pointed out that an upper LL cutoff of $N_c \sim 25\phi_0/\phi$ is needed to faithfully reproduce the narrow-band Hofstadter spectrum of TBG, where $\phi_0 = hc/e$ is the magnetic flux quantum and $\phi$ is the magnetic flux per moiré unit cell. This is a computationally intensive procedure, especially at low $\mathbf{B}$ when $N_c$ becomes large. In the second approach, the magnetic field effects are accounted for via Peierls substitution, i.e., by replacing the intersite hopping amplitude $t_{ij}$ with $t_{ij}\exp[-i\frac{e}{\hbar c}\int_{\mathbf{r}_i}^{\mathbf{r}_j} d\mathbf{r}\cdot\mathbf{A}(\mathbf{r})]$. The Peierls substitution has been used extensively in the literature due to its simplicity in addressing Hofstadter physics. However, it is unclear how to generalize the Peierls substitution to a subset of Bloch bands where 2D exponentially localized and symmetric Wannier orbitals cannot be constructed [43–45].

In our earlier work [46], to address the Hofstadter physics in TBG, we proposed a procedure for constructing the narrow-band Hilbert space at a rational magnetic flux ratio $\phi/\phi_0 = p/q$ by projecting the zero-field hybrid Wannier basis states (hWSs) onto eigenstates of the magnetic translation group (MTG). Such hWSs are Bloch extended along one direction and exponentially localized along the other and can always be constructed without topological obstruction [47–49]. The pair of hWSs within a valley of TBG carries ±1 Chern numbers, which are manifested in the intra-moiré-unit-cell shift of the averaged position along the localization direction when the Bloch wave number along the extended direction is changed [50]. We demonstrated that the wave functions generated from this projection procedure have a good overlap with the exact

*xiaoyuw@magnet.fsu.edu
†vafek@magnet.fsu.edu

 ©2023 American Physical Society

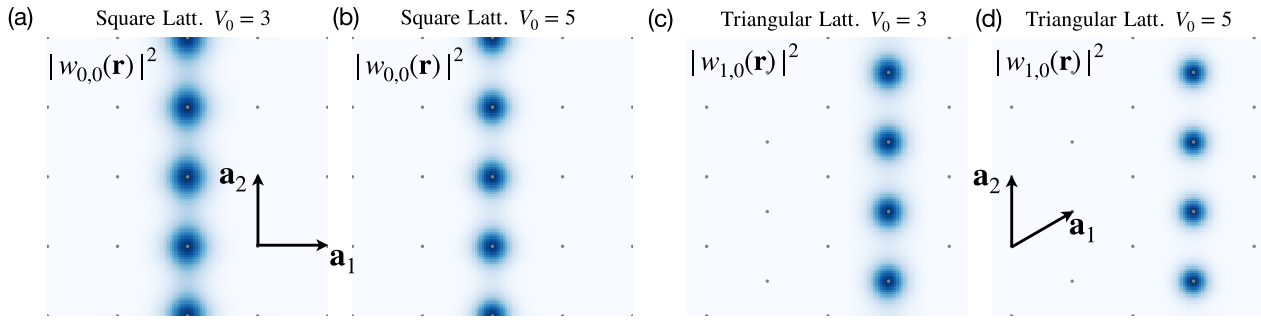


FIG. 1. Hybrid Wannier states $w_{n_0,k_2}(\mathbf{r})$ of the lowest-energy Bloch band for (a) and (b) a square lattice and (c) and (d) triangular lattice potential. In both cases we used the potential $V(\mathbf{r}) = -V_0 \sum_{\mathbf{g}} e^{i\mathbf{g}\cdot\mathbf{r}}$. We set $\hbar^2/m_e a^2 = 1$, where $m_e$ is the bare electron mass and $a$ is the lattice constant. For the square lattice, $\mathbf{g} = \pm\mathbf{g}_1, \pm\mathbf{g}_2$, whereas for the triangular lattice, $\mathbf{g} = \pm\mathbf{g}_1, \pm\mathbf{g}_2, \pm(\mathbf{g}_1 + \mathbf{g}_2)$. The states are well localized on the lattice sites, and their spatial support narrows with increasing lattice potential strength.

wave functions obtained using the LL approach at low **B** while being a much more efficient numerical procedure than the LL approach for addressing interaction effects [46].

In this work, we present a detailed discussion of the procedure developed in Ref. [46] and apply it to revisit the noninteracting Hofstadter spectra for square and triangular lattice potentials, where the lowest-energy Bloch bands at zero field are topologically trivial. We make quantitative comparisons to the exact LL approach to demonstrate the projection method's regime of validity, as well as derive the Peierls substitution and Harper equation studied extensively in the literature. This paper is organized as follows: In Sec. II we briefly discuss the LL approach and MTG eigenstates. In Sec. III we elaborate on the hWSs and how to construct a complete and orthonormal set of MTG eigenstates for a subset of Bloch bands at a finite magnetic field. We derive the Peierls substitution as a limiting case when the magnetic length [defined below Eq. (1)] is much longer than the spatial support of the hWS, and we rederive the Harper equation directly using the hWS approach. A summary is provided in Sec. IV.

## II. LANDAU LEVEL APPROACH

We begin with a brief review of the LL approach for addressing the magnetic field effects on electrons moving in a 2D periodic lattice potential. For notational convenience, we introduce the two lattice vectors as $\mathbf{a}_1$ and $\mathbf{a}_2$ and the two reciprocal lattice vectors as $\mathbf{g}_1$ and $\mathbf{g}_2$. They satisfy the relation $\mathbf{a}_i \cdot \mathbf{g}_j = 2\pi\delta_{ij}$. For a generic 2D lattice $\mathbf{a}_1$ and $\mathbf{a}_2$ are not required to be orthogonal [see, e.g., Fig. 1(d)]. We further work with the Landau gauge $\mathbf{A} = Bx\mathbf{e}_y$, where $B$ is the magnetic field in the out-of-plane $\mathbf{e}_z$ direction and $\mathbf{e}_y$ ($\mathbf{e}_x$) is along the direction parallel (perpendicular) to $\mathbf{a}_2$; $\mathbf{e}_{i=x,y,z}$ are unit vectors. The LL wave functions are given by

$$|\psi_n(k_y)\rangle = \frac{1}{\sqrt{N_2 a_2}} e^{ik_y y} \hat{T}(-k_y \ell^2 \mathbf{e}_x)|n\rangle, \tag{1}$$

where $N_2 a_2$ is the length of the system along the $\mathbf{e}_y$ direction, $\ell \equiv \sqrt{\frac{\hbar c}{eB}}$ is the magnetic length, $k_y \in \mathbb{R}$ is the momentum quantum number such that $\hat{p}_y|\psi_n(k_y)\rangle = \hbar k_y|\psi_n(k_y)\rangle$, and $|n\rangle$ is the $n$th eigenstate for a 1D harmonic oscillator,

$$\langle \mathbf{r}|n\rangle = \frac{1}{\pi^{1/4}\sqrt{2^n n!}} e^{-\frac{x^2}{2\ell^2}} H_n\left(\frac{x}{\ell}\right), \tag{2}$$

where $H_n(x)$ is the Hermite polynomial. The operator $\hat{T}(\mathbf{r}_0) = e^{-i\mathbf{r}_0\cdot\hat{\mathbf{p}}/\hbar}$ generates a translation by $-\mathbf{r}_0$; that is, for a general function $f(\mathbf{r})$ we have

$$\hat{T}(\mathbf{r}_0) f(\mathbf{r}) = f(\mathbf{r} - \mathbf{r}_0). \tag{3}$$

The LL degeneracy argument proceeds as usual: consider a system of area $N_1\mathbf{a}_1 \times N_2\mathbf{a}_2$, such that it extends along $\mathbf{a}_{i=1,2}$ by $N_{i=1,2} \in \mathbb{Z}$ unit cells. For open boundary conditions along $\mathbf{a}_1$, the quantum number $k_y$ must satisfy $(k_y\ell^2)_{\max} - (k_y\ell^2)_{\min} = N_1 a_{1x}$. For periodic boundary condition along $\mathbf{a}_2$, the separation between adjacent wave vectors is $\delta k_y = \frac{2\pi}{N_2 a_2}$. The total LL degeneracy is then $\mathcal{N} = [(k_y)_{\max} - (k_y)_{\min}]/\delta k_y = (N_1 N_2)\frac{|\mathbf{a}_1\times\mathbf{a}_2|}{2\pi\ell^2}$, or equivalently, the LL degeneracy per unit cell is given as

$$\frac{\mathcal{N}}{N_1 N_2} = \frac{\phi}{\phi_0}, \tag{4}$$

where $\phi_0 = hc/e$ is the magnetic flux quantum and $\phi = B|\mathbf{a}_1 \times \mathbf{a}_2|$ is the magnetic flux through a unit cell.

### A. Eigenstates of the magnetic translation group

The single-electron Hamiltonian $\hat{H}(\mathbf{r}, \hat{\mathbf{p}} + \frac{e}{c}\mathbf{A})$ is invariant under discrete magnetic translations $[\hat{H}, \hat{t}(\mathbf{a}_i)] = 0$, where $\hat{t}(\mathbf{a}_{i=1,2})$ are discrete magnetic translation operators along the $\mathbf{a}_{i=1,2}$ directions. In the Landau gauge, they are given as

$$\hat{t}(\mathbf{a}_1) = e^{-i\mathbf{q}_\phi\cdot\mathbf{r}}\hat{T}(\mathbf{a}_1), \tag{5}$$

$$\hat{t}(\mathbf{a}_2) = \hat{T}(\mathbf{a}_2), \tag{6}$$

where we define the wave vector associated with magnetic scattering as

$$\mathbf{q}_\phi = \frac{2\pi}{a_2}\frac{\phi}{\phi_0}\mathbf{e}_y = \frac{a_{1x}}{\ell^2}\mathbf{e}_y. \tag{7}$$

These operators satisfy

$$\hat{t}(\mathbf{a}_2)\hat{t}(\mathbf{a}_1) = e^{i2\pi\frac{\phi}{\phi_0}}\hat{t}(\mathbf{a}_1)\hat{t}(\mathbf{a}_2). \tag{8}$$

Therefore, if $\phi/\phi_0 = p/q$, where $p$ and $q$ are coprime integers,

$$[\hat{t}(\mathbf{a}_1), \hat{t}^q(\mathbf{a}_2)] = 0. \tag{9}$$

As a result, eigenstates of $\hat{H}(\mathbf{r}, \hat{\mathbf{p}} + \frac{e}{c}\mathbf{A})$ can be chosen to be simultaneous eigenstates of $\hat{t}(\mathbf{a}_1)$ and $\hat{t}^q(\mathbf{a}_2)$.

It is straightforward to show that a complete and orthonormal set of MTG basis states can be constructed from the LL wave functions as

$$|\Psi_{n,r}(\mathbf{k})\rangle = \frac{1}{\sqrt{N}} \sum_{s=-\infty}^{\infty} e^{i2\pi k_1 s} \hat{t}^s(\mathbf{a}_1) \left| \psi_n\left(\frac{2\pi}{a_2}\left(k_2 + \frac{r}{q}\right)\right)\right\rangle, \tag{10}$$

where $N$ is a normalization factor. The wave vector $\mathbf{k} = k_1\mathbf{g}_1 + k_2\mathbf{g}_2$ resides in the magnetic Brillouin zone, defined as $k_1 \in [0, 1)$ and $k_2 \in [0, \frac{1}{q})$, and the integer $r$ labels the magnetic strip $[\frac{r-1}{q}, \frac{r}{q})$ along the $\mathbf{g}_2$ direction. The independent basis states are defined for $r = 0, \ldots, p-1$ because (see Appendix A)

$$|\Psi_{n,r+p}(\mathbf{k})\rangle = e^{i2\pi(k_1 - (k_2 + \frac{r+p}{q})\frac{a_{1y}}{a_2})}|\Psi_{n,r}(\mathbf{k})\rangle. \tag{11}$$

It is straightforward to check that the states in Eq. (10) are MTG eigenstates, i.e.,

$$\hat{t}(\mathbf{a}_1)|\Psi_{n,r}(\mathbf{k})\rangle = e^{-i2\pi k_1}|\Psi_{n,r}(\mathbf{k})\rangle, \tag{12}$$

$$\hat{t}^q(\mathbf{a}_2)|\Psi_{n,r}(\mathbf{k})\rangle = e^{-i2\pi q k_2}|\Psi_{n,r}(\mathbf{k})\rangle. \tag{13}$$

They also satisfy the orthonormality condition:

$$\langle\Psi_{n_1,r_1}(\mathbf{k})|\Psi_{n_2,r_2}(\mathbf{p})\rangle = \delta_{n_1,n_2}\delta_{r_1,r_2}\delta_{\mathbf{k},\mathbf{p}}. \tag{14}$$

In the absence of a periodic lattice potential, the LL degeneracy per unit cell is given by $p \times 1 \times \frac{1}{q}$, consistent with Eq. (4). Here $p$ comes from the degeneracy of quantum number $r$, and a fully occupied magnetic Brillouin zone corresponds to $1 \times \frac{1}{q}$ of the zero-field Brillouin zone being occupied, i.e., the fraction of one particle per unit cell.

Note that $\hat{t}(\mathbf{a}_2)$ acts nontrivially on the LL-based MTG eigenstates, and because

$$\hat{t}(\mathbf{a}_2)|\Psi_{n,r}(\mathbf{k})\rangle = e^{-i2\pi(k_2 + \frac{r}{q})}\left|\Psi_{n,r}\left(\mathbf{k} + \frac{p}{q}\mathbf{g}_1\right)\right\rangle, \tag{15}$$

$\hat{t}(\mathbf{a}_2)|\Psi_{n,r}(\mathbf{k})\rangle$ is an MTG eigenstate at wave vector $\mathbf{k} + \frac{p}{q}\mathbf{g}_1$.

Without loss of clarity, from now on for convenience we use $|\psi_n(k_2 + \frac{r}{q})\rangle$ to denote a LL wave function with wave number $\frac{2\pi}{a_2}(k_2 + \frac{r}{q})$.

### B. Matrix elements of the Hamiltonian

We study the matrix elements of the continuum single-electron Hamiltonian given by

$$\hat{H}\left(\mathbf{r}, \hat{\mathbf{p}} + \frac{e}{c}\mathbf{A}\right) = \frac{\left(\hat{\mathbf{p}} + \frac{e}{c}\mathbf{A}\right)^2}{2m_e} + V(\mathbf{r}), \tag{16}$$

where $e > 0$ is the electric charge and $V(\mathbf{r}) = \sum_{\mathbf{g}} V_{\mathbf{g}} e^{i\mathbf{g}\cdot\mathbf{r}}$ is the periodic lattice potential, where $\mathbf{g} = m\mathbf{g}_1 + n\mathbf{g}_2$ are reciprocal lattice vectors, with $m, n \in \mathbb{Z}$.

The matrix elements of the kinetic energy in the LL-based MTG eigenstate basis [Eq. (10)] can be straightforwardly calculated by rewriting $\hat{\pi}_x = \frac{\hbar}{\sqrt{2}\ell}(a + a^\dagger)$ and $\hat{\pi}_y = \frac{\hbar}{i\sqrt{2}\ell}(a^\dagger - a)$, where $\hat{\vec{\pi}} = \hat{\mathbf{p}} + \frac{e}{c}\mathbf{A}$ is the canonical momentum and $a$ is the harmonic oscillator lowering operator.

The matrix elements of a general operator of the form $\hat{O}_{\mathbf{q}} = \mathcal{O}_{\mathbf{q}} e^{i\mathbf{q}\cdot\mathbf{r}}$ can be calculated as follows [46]:

$$\begin{aligned}(\hat{O}_{\mathbf{q}})_{nr_1,mr_2}(\mathbf{k},\mathbf{p}) &\equiv \langle\Psi_{n,r_1}(\mathbf{k})|\hat{O}_{\mathbf{q}}|\Psi_{m,r_2}(\mathbf{p})\rangle \\ &= \mathcal{O}_{\mathbf{q}}\delta_{p_1,[k_1-q_1]_1}\sum_{s=-\infty}^{\infty}\delta_{\tilde{p}_y - sq_\phi, \tilde{k}_y - q_y} e^{i2\pi p_1 s} e^{-is\tilde{p}_y a_{1y}} e^{i\frac{s(s-1)}{2}\mathbf{q}_\phi\cdot\mathbf{a}_1} e^{-iq_x\tilde{k}_y\ell^2} e^{\frac{i}{2}q_x q_y \ell^2}\langle n|e^{c_- a + c_+ a^\dagger}|m\rangle,\end{aligned} \tag{17}$$

where we define $c_\pm = i\frac{\ell}{\sqrt{2}}(q_x \mp iq_y)$ and

$$\tilde{\mathbf{k}} = \mathbf{k} + \frac{r_1}{q}\mathbf{g}_2, \ \tilde{\mathbf{p}} = \mathbf{p} + \frac{r_2}{q}\mathbf{g}_2. \tag{18}$$

$\tilde{k}_y$ and $\tilde{p}_y$ are defined as $\tilde{\mathbf{k}}\cdot\mathbf{e}_y$ and $\tilde{\mathbf{p}}\cdot\mathbf{e}_y$, respectively. The notation $[b]_a$ represents $b$ modulo $a$, with $a > 0$. The expression in the last line is calculated as

$$\langle n|e^{c_- a + c_+ a^\dagger}|m\rangle = \begin{cases} e^{\frac{1}{2}c_+c_-}\sqrt{\frac{m!}{n!}}(c_+)^{n-m}L_m^{n-m}(-c_+c_-) & \text{for } n \geqslant m, \\ e^{\frac{1}{2}c_+c_-}\sqrt{\frac{n!}{m!}}(c_-)^{m-n}L_n^{m-n}(-c_+c_-) & \text{for } n < m, \end{cases} \tag{19}$$

where

$$L_n^k(x) = \sum_{m=0}^{n}(-x)^m\frac{(n+k)!}{(n-m)!(k+m)!m!}$$

is the associated Laguerre polynomial. Note that any operator of the form $e^{i\mathbf{q}\cdot\mathbf{r}}$ is a dense matrix in the LL indices $\{m, n\}$. This poses numerical challenges at low magnetic flux ratios when the upper LL cutoff is large.

The eigenstates and eigenenergies of the single-electron Hamiltonian in a magnetic field and periodic lattice potential can now be solved by diagonalizing the matrix Hamiltonian in the LL-based MTG basis. We briefly discuss the degeneracy of energy levels. Consider an energy eigenstate at a momentum $\mathbf{k}$ inside the magnetic Brillouin zone, such that

$$\hat{H}|\tilde{\Psi}_n(\mathbf{k})\rangle = \varepsilon_{n,\mathbf{k}}|\tilde{\Psi}_n(\mathbf{k})\rangle. \tag{20}$$

Making use of the magnetic translation operator $\hat{t}(\mathbf{a}_2)$, we observe that

$$\hat{H}(\hat{t}(\mathbf{a}_2)|\tilde{\Psi}_n(\mathbf{k})\rangle) = \hat{t}(\mathbf{a}_2)\hat{H}|\tilde{\Psi}_n(\mathbf{k})\rangle = \varepsilon_{n,\mathbf{k}}(\hat{t}(\mathbf{a}_2)|\tilde{\Psi}_n(\mathbf{k})\rangle). \quad (21)$$

The state $\hat{t}(\mathbf{a}_2)|\tilde{\Psi}_n(\mathbf{k})\rangle$ is therefore also an energy eigenstate at $\varepsilon_{n,\mathbf{k}}$, but at the wave vector $\mathbf{k} + \frac{p}{q}\mathbf{g}_1$. As a result each energy level is at least $q$-fold degenerate, and therefore, the dispersion of the resulting magnetic subbands is effectively restricted to the wave vector domain $[0, \frac{1}{q}) \times [0, \frac{1}{q})$.

The LL approach is an exact method, limited in practice only by the truncation of the upper LL index. In the free electron case, retaining $N_c$ LLs allows an accurate representation of the energetics up to $W \approx \frac{1}{\lambda} N_c \frac{\hbar^2}{m_e \ell^2}$, where $\lambda > 1$ is a parameter dependent on the strength of the lattice potential, as discussed in the Introduction. In the low-field limit, the LLs become dense, and a larger LL index is therefore necessary to describe the magnetic subbands emanating from the $\mathbf{B} = 0$ Bloch bands up to the energy $W$. This makes the LL approach both inefficient and not intuitive to study the low-field physics, and an alternative approach that bridges the zero-field and finite-field Hilbert space is preferable. As we show in the next section, this is achieved by projecting the hWSs, which form the basis of the $\mathbf{B} = 0$ Hilbert space, onto representations of the MTG.

## III. HYBRID WANNIER APPROACH

### A. Hybrid Wannier states at B = 0

In the absence of the magnetic field, the energy eigenstates are given by the Bloch states

$$\psi_{n,\mathbf{k}}(\mathbf{r}) = \frac{1}{\sqrt{\mathcal{A}}} e^{i\mathbf{k}\cdot\mathbf{r}} u_{n,\mathbf{k}}(\mathbf{r}), \quad (22)$$

where $\mathcal{A}$ is the area of the 2D system, $n$ is the band label, $\mathbf{k} = k_1\mathbf{g}_1 + k_2\mathbf{g}_2$ is the crystal momentum in the first Brillouin zone (for convenience we choose it to be $k_1, k_2 \in [0, 1) \times [0, 1)$), and $u_{n,\mathbf{k}}(\mathbf{r})$ is periodic under discrete lattice translations $\hat{T}(\mathbf{a}_{i=1,2})$. The notation $\psi_{n,\mathbf{k}}(\mathbf{r})$ should not be confused with the LL wave functions discussed in the previous section. One can construct spatially localized basis states by performing unitary transformations on the (extended) Bloch energy eigenstates. For a subset of Bloch bands of interest, we can construct hWSs from the Bloch states even if these bands have nontrivial topology, provided that the gap to the adjacent bands does not close. hWSs are exponentially localized in one direction (say, $\mathbf{a}_1$) and Bloch extended along the other (say, $\mathbf{a}_2$). In Fig. 1 we show several examples of hWSs for the lowest-energy Bloch band on square and triangular lattices. These states can be constructed [48,50] by diagonalizing the periodic version of the position operator $\exp(i\delta\mathbf{k}\cdot\mathbf{r})$ projected onto the Bloch basis from the desired energy bands, where $\delta\mathbf{k} = \frac{1}{N_1}\mathbf{g}_1$ hybridizes Bloch states at $\mathbf{k}$ and $\mathbf{k} + \delta\mathbf{k}$. The resulting hWS that is exponentially localized near a column at $n_0\mathbf{a}_1$ can be expressed as

$$|w_\alpha(n_0, k_2)\rangle = \frac{1}{\sqrt{N_1}} \sum_{n\in\text{subset}} \sum_{k_1} e^{-i2\pi k_1 n_0} U_{n,\alpha}(\mathbf{k})|\psi_{n,\mathbf{k}}\rangle, \quad (23)$$

where the summation over $n$ is over a subset of Bloch bands of interest and $U(\mathbf{k})$ is a unitary matrix at every $\mathbf{k}$. Under discrete translations the hWSs satisfy

$$\hat{T}(\mathbf{a}_1)|w_\alpha(n_0, k_2)\rangle = |w_\alpha(n_0 + 1, k_2)\rangle, \quad (24)$$

$$\hat{T}(\mathbf{a}_2)|w_\alpha(n_0, k_2)\rangle = e^{-i2\pi k_2}|w_\alpha(n_0, k_2)\rangle. \quad (25)$$

For topologically nontrivial bands, the hWSs contain information about the nonzero Chern number of the Bloch band, which is manifested in the nontrivial evolution of the averaged position $\langle\mathbf{r}\cdot\mathbf{g}_1\rangle/|\mathbf{g}_1|$ within the hWSs when $k_2$ is continuously increased from 0 to 1. One example of such hWSs is the pair of narrow bands in TBG for a given valley and spin. For more details we refer interested readers to Refs. [46,50].

### B. MTG eigenstates from hybrid Wannier states

The set of hWSs for all Bloch bands forms a complete basis even in finite magnetic field. However, it is not useful if we are interested in only the Hofstadter physics of a subset of Bloch bands.

It is tempting, but wrong, to take the subset of the $\mathbf{B} = 0$ Bloch bands as a basis of the corresponding subset of the $\mathbf{B} \neq 0$ states. Note that the correct projector at $\mathbf{B} \neq 0$, $\hat{P}_B = \sum_n' \sum_{\mathbf{k}} |\tilde{\Psi}_n(\mathbf{k})\rangle\langle\tilde{\Psi}_n(\mathbf{k})|$ [see Eq. (20)], where $n$ is summed over the subset of magnetic subbands of interest, is invariant under any integer multiple of magnetic translations, i.e., $[\hat{P}_B, \hat{t}^{s_1}(\mathbf{a}_1)\hat{t}^{s_2}(\mathbf{a}_2)] = 0$, where $s_1, s_2 \in \mathbb{Z}$. However, the $\mathbf{B} = 0$ projector, $\hat{P} = \sum_{n\in\text{subset}} \sum_{\mathbf{k}} |\psi_{n,\mathbf{k}}\rangle\langle\psi_{n,\mathbf{k}}|$, is not invariant under $\hat{t}^{s_1}(\mathbf{a}_1)$ because

$$\hat{t}^{s_1}(\mathbf{a}_1)\hat{P}\hat{t}^{-s_1}(\mathbf{a}_1) = \sum_{mm'\in\text{fullset}} \sum_{\mathbf{k}} |\psi_{m,\mathbf{k}}\rangle\langle\psi_{m',\mathbf{k}}| \sum_{n\in\text{subset}} U_{mn}(\mathbf{k})U^\dagger_{nm'}(\mathbf{k}). \quad (26)$$

Here we define

$$\hat{t}^{s_1}(\mathbf{a}_1)|\psi_{n,\mathbf{k}}\rangle = \sum_{m\in\text{fullset}} U_{mn}(\mathbf{k})|\psi_{m,\mathbf{k}}\rangle. \quad (27)$$

Due to the restriction on $n$, the right-hand side of Eq. (26) is not equal to $\hat{P}$, the narrow-band projector at $\mathbf{B} = 0$. In other words, the $y$-dependent phase in $\hat{t}(\mathbf{a}_1)$ takes the states outside of the subset of the zero-field bands of interest. This problem is severe even at low $\mathbf{B}$ for sufficiently large $s_1$. Therefore, $\hat{P}$ is *not* a projector onto the states of interest in finite magnetic fields.

In order to construct the correct finite-field Hilbert space, we first construct MTG eigenstates from the hWSs,

$$|W_{\alpha,r}(\mathbf{k})\rangle = \frac{1}{\sqrt{N_1}} \sum_{s=-\frac{N_1}{2}}^{\frac{N_1}{2}} e^{i2\pi k_1 s}\hat{t}^s(\mathbf{a}_1)\left|w_\alpha\left(0, k_2 + \frac{r}{q}\right)\right\rangle. \quad (28)$$

Unlike in Sec. III A, here $k_2 \in [0, \frac{1}{q})$, and $r = 0, \ldots, q-1$. The choice of hWSs at $n_0 = 0$ is motivated by the fact that the vector potential in the Landau gauge vanishes at the origin. Therefore, $|w_\alpha(0, k_2 + \frac{r}{q})\rangle$ must have a large overlap with the subset of the $\mathbf{B} \neq 0$ Hilbert space with similar energy at small $B$, i.e., with the magnetic subbands emanating from the $\mathbf{B} = 0$

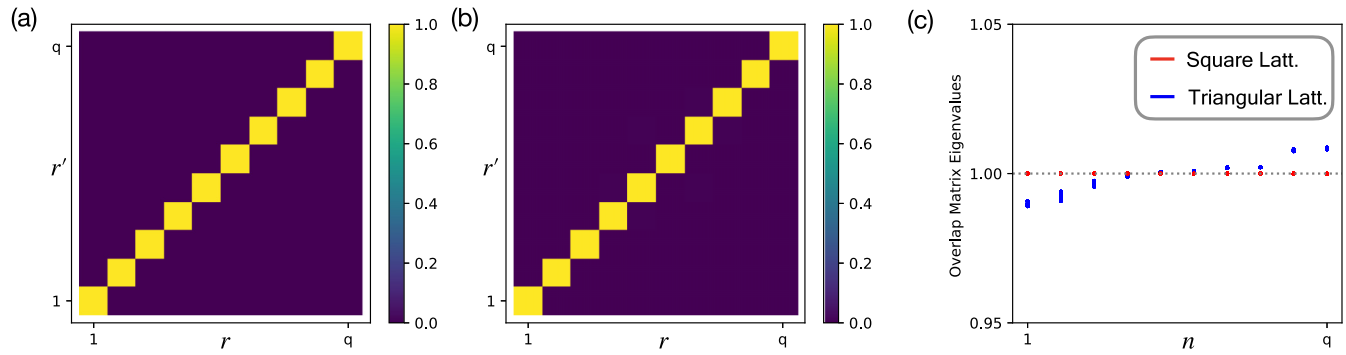


FIG. 2. Typical absolute value of the matrix elements of the overlap matrix [Eq. (32)], calculated at flux $\phi/\phi_0 = 1/10$ for (a) square and (b) triangular lattice potentials with $V_0 = 3$. We set the energy scale $\hbar^2/m_e a^2 = 1$. (c) Eigenvalues of the overlap matrix. The axes in (a) and (b) correspond to the basis indices $r$ and $r'$, and in (c) they correspond to the ordered eigenvalue index. If the MTG basis states generated from hWSs constitute a complete and orthonormal basis, the overlap matrix is an identity matrix, and all eigenvalues are equal to 1. While this is true for the square lattice potential, there are small deviations from orthonormality for the case of the triangular lattice potential. As a result a further orthonormalization procedure is needed, as outlined in the text.

bands of interest. The rest of the basis can be conveniently obtained by using the magnetic translation operator which moves hWSs along the $\mathbf{a}_1$ direction while also attaching a phase due to the vector potential.

It is straightforward to check that $|W_{\alpha,r}(\mathbf{k})\rangle$ are, indeed, MTG eigenstates, i.e.,

$$\hat{t}(\mathbf{a}_1)|W_{\alpha,r}(\mathbf{k})\rangle = e^{-i2\pi k_1}|W_{\alpha,r}(\mathbf{k})\rangle, \tag{29}$$

$$\hat{t}^q(\mathbf{a}_2)|W_{\alpha,r}(\mathbf{k})\rangle = e^{-i2\pi q k_2}|W_{\alpha,r}(\mathbf{k})\rangle. \tag{30}$$

To address the completeness and orthonormality of the wave functions defined in Eq. (28), we define an overlap matrix

$$\Lambda_{\alpha r_1,\beta r_2}(\mathbf{k}) \equiv \langle W_{\alpha,r_1}(\mathbf{k})|W_{\beta,r_2}(\mathbf{k})\rangle. \tag{31}$$

Note that states with different $\mathbf{k}$ are automatically orthogonal due to different eigenvalues under $\hat{t}(\mathbf{a}_{i=1,2})$. If these wave functions represent a complete and orthonormal set, the overlap matrix should be an identity matrix. The overlap matrix can be calculated as follows:

$$\begin{aligned}\Lambda_{\alpha r_1,\beta r_2}(\mathbf{k}) &= \sum_s e^{i2\pi k_1 s}\langle w_\alpha\left(0, k_2 + \frac{r_1}{q}\right)|\hat{t}^s(\mathbf{a}_1)\left|w_\beta\left(0, k_2 + \frac{r_2}{q}\right)\right\rangle \\ &= \sum_s e^{i2\pi k_1 s} e^{i\frac{s(s-1)}{2}\mathbf{q}_\phi\cdot\mathbf{a}_1}\langle w_\alpha(0,\tilde{k}_2)|e^{-is\mathbf{q}_\phi\cdot\mathbf{r}}|w_\beta(s,\tilde{p}_2)\rangle,\end{aligned} \tag{32}$$

where in the second line we define $\tilde{k}_2 = k_2 + \frac{r_1}{q}$ and $\tilde{p}_2 = k_2 + \frac{r_2}{q}$ $(\tilde{k}_2, \tilde{p}_2 \in [0,1))$ and use the operator identity in Eq. (A1).

If the hWSs represent topologically trivial Bloch bands (e.g., Fig. 1), the overlap of two hWSs is exponentially suppressed unless they have the same localization center, i.e., unless $s = 0$ in Eq. (32). Therefore, $\langle W_{\alpha,r_1}(\mathbf{k})|W_{\beta,r_2}(\mathbf{p})\rangle \approx \delta_{\alpha,\beta}\delta_{\mathbf{k},\mathbf{p}}\delta_{r_1,r_2}$ with exponential accuracy. This is illustrated in Fig. 2 for the square and triangular lattice potentials. Even if $\Lambda(\mathbf{k})$ is not an identity matrix, a complete and orthonormal basis set can be generated by eigendecomposition, $U^\dagger \Lambda U = D$, and redefining a new set of basis states as

$$|V_a(\mathbf{k})\rangle = \sum_{\alpha,r}|W_{\alpha,r}(\mathbf{k})\rangle\left(U\frac{1}{\sqrt{D}}\right)_{\alpha r,a}. \tag{33}$$

If hWSs represent topological bands with finite Chern numbers, hWSs with different localization centers have a finite spatial overlap, and the overlap matrix in Eq. (32) strongly deviates from an identity matrix. Importantly, as discussed in Ref. [46], for hWSs with Chern numbers $\pm 1$, the number of independent MTG eigenstates should increase or decrease according to the Streda formula. This manifests in the rank deficiency of the overlap matrix. A procedure that makes use of a different choice of the localization center $n_0$ (still close to zero where the $\mathbf{A}$ is small) was proposed in Ref. [46], where it was shown to resolve this issue.

The next question is how well these basis states describe the finite-field Hilbert space of interest. To quantify the amount of spillover into remote magnetic subbands, we can expand Eq. (33) in the exact wave functions obtained based on the LL approach,

$$|V_a(\mathbf{k})\rangle = \sum_{n\in\text{active}} M_{n,a}(\mathbf{k})|\tilde{\Psi}_n(\mathbf{k})\rangle + \sum_{n'\in\text{remote}} M_{n',a}(\mathbf{k})|\tilde{\Psi}_{n'}(\mathbf{k})\rangle, \tag{34}$$

where $|\tilde{\Psi}_n(\mathbf{k})\rangle$ are the exact eigenstates obtained from the LL approach and $M_{n,a}(\mathbf{k})$ are the expansion coefficients. Define

$$\eta_a \equiv \frac{1}{N_1}\frac{1}{N_2/q}\sum_{\mathbf{k}}\sum_{n'\in\text{remote}}|M_{n',a}(\mathbf{k})|^2. \tag{35}$$

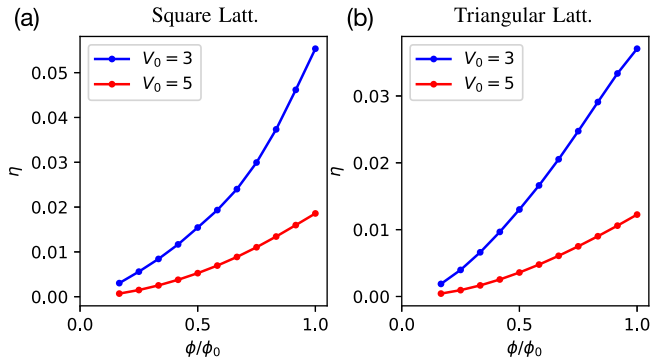


FIG. 3. The amount of spillover $\eta$ of MTG basis states into the Hilbert space of remote Hofstadter bands for square and triangular lattice potentials. We set the energy scale $\hbar^2/m_e a^2 = 1$. The spillover decreases with increasing lattice potential strength and increases with increasing magnetic flux.

Then $\eta_a \in [0, 1]$ characterizes the amount of spillover into remote magnetic subbands. In Fig. 3 we plot $\eta = \eta_{a=1}$ versus $\phi/\phi_0$ for the lowest-energy Bloch band for square and triangular lattice potentials. The amount of spillover decreases with increasing strength of the lattice potential and remains small even for reasonably large magnetic flux.

### C. Peierls factor and MTG basis states

To gain better insight into the MTG basis states obtained from zero-field hWSs, let us consider an example of an isolated and topologically trivial band, where 2D Wannierization can be achieved. The hWSs are related to 2D Wannier orbitals via Fourier transform along the $\mathbf{a}_2$ axis, i.e.,

$$\langle \mathbf{r}|w(n_0, k_2)\rangle = \frac{1}{\sqrt{N_2}} \sum_{\mathbf{R}} \phi_{\mathbf{R}}(\mathbf{r}) \delta_{\mathbf{R}\cdot\mathbf{g}_1, 2\pi n_0} e^{ik_2 \mathbf{g}_2\cdot\mathbf{R}}. \tag{36}$$

$\phi_{\mathbf{R}}(\mathbf{r})$ denotes a 2D localized Wannier orbital at site $\mathbf{R} = m\mathbf{a}_1 + n\mathbf{a}_2$, with the normalization condition $\int \mathrm{d}^2\mathbf{r}\phi^*_{\mathbf{R}}(\mathbf{r})\phi_{\mathbf{R}'}(\mathbf{r}) = \delta_{\mathbf{R},\mathbf{R}'}$. The MTG basis states can then be written as

$$\langle \mathbf{r}|W_r(\mathbf{k})\rangle = \frac{1}{\sqrt{N_1 N_2}} \sum_{\mathbf{R}} e^{i\tilde{\mathbf{k}}\cdot\mathbf{R}} \hat{t}^m(\mathbf{a}_1)\hat{t}^n(\mathbf{a}_2)\phi_{\mathbf{0}}(\mathbf{r}), \tag{37}$$

where we define $\tilde{\mathbf{k}} = k_1\mathbf{g}_1 + (k_2 + \frac{r}{q})\mathbf{g}_2$. Compared to the zero-field Bloch states, the MTG states are obtained by acting on the 2D Wannier orbital at site $\mathbf{R} = \mathbf{0}$ with noncommuting magnetic translation operators instead of the usual lattice translation operators.

We make a connection to the Peierls factor used in the literature [40], where the phase $\exp[-i\frac{e}{\hbar c}\int_{\mathbf{R}}^{\mathbf{r}} \mathrm{d}\mathbf{r}'\cdot\mathbf{A}(\mathbf{r}')]$ is attached to the 2D ($\mathbf{B} = 0$) Wannier orbital $\phi_{\mathbf{R}}(\mathbf{r})$ with the integration along the straight line from $\mathbf{R}$ to $\mathbf{r}$. Expanding out the magnetic translation operators in Eq. (37),

$$\langle \mathbf{r}|W_r(\mathbf{k})\rangle = \frac{1}{\sqrt{N_1 N_2}} \sum_{\mathbf{R}} e^{i\tilde{\mathbf{k}}\cdot\mathbf{R}} e^{i\frac{m(m-1)}{2}\mathbf{q}_\phi\cdot\mathbf{a}_1} e^{-im\mathbf{q}_\phi\cdot\mathbf{r}} \phi_{\mathbf{R}}(\mathbf{r}). \tag{38}$$

If the Wannier orbitals are exponentially localized near the lattice sites and the magnetic length is much longer than their spatial extent, then we can take $|\mathbf{r} - \mathbf{R}|/\ell \ll 1$ and approximate

$$e^{-im\mathbf{q}_\phi\cdot\mathbf{r}}\phi_{\mathbf{R}}(\mathbf{r}) \approx e^{-im\mathbf{q}_\phi\cdot\mathbf{R}}[e^{-i\frac{e}{\hbar c}\int_{\mathbf{R}}^{\mathbf{r}}\mathrm{d}\mathbf{r}'\cdot\mathbf{A}(\mathbf{r}')}\phi_{\mathbf{R}}(\mathbf{r})], \tag{39}$$

where we used

$$\begin{aligned} & i\frac{e}{\hbar c}\int_{\mathbf{R}}^{\mathbf{r}} \mathrm{d}\mathbf{r}'\cdot\mathbf{A}(\mathbf{r}') \\ &= \frac{i}{\ell^2}R_x(y - R_y) + \frac{i}{2\ell^2}(x - R_x)(y - R_y) \\ &= im\frac{a_{1x}}{\ell^2}(y - R_y) + \frac{i}{2\ell^2}(x - R_x)(y - R_y) \\ &= im\mathbf{q}_\phi\cdot(\mathbf{r} - \mathbf{R}) + O(|\mathbf{r} - \mathbf{R}|^2/\ell^2). \end{aligned} \tag{40}$$

This explicitly demonstrates the link between the MTG basis states and the Wannier orbitals with a Peierls factor.

### D. Matrix elements of the Hamiltonian

Here we work out the matrix elements of the single-electron Hamiltonian in the MTG basis states defined in Eq. (28). Matrix elements with respect to the orthonormal basis $|V_a(\mathbf{k})\rangle$ can be obtained via the basis transformation in Eq. (33). Specifically,

$$\begin{aligned} & \langle W_{\alpha,r_1}(\mathbf{k})|\hat{H}|W_{\beta,r_2}(\mathbf{k})\rangle \\ &= \sum_s e^{i2\pi k_1 s} e^{i\frac{s(s-1)}{2}\mathbf{q}_\phi\cdot\mathbf{a}_1} \langle w_\alpha(0, \tilde{k}_2)|\hat{H}e^{-is\mathbf{q}_\phi\cdot\mathbf{r}}|w_\beta(s, \tilde{p}_2)\rangle, \end{aligned} \tag{41}$$

where we define $\tilde{k}_2 = k_2 + \frac{r_1}{q}$ and $\tilde{p}_2 = k_2 + \frac{r_2}{q}$ ($\tilde{k}_2, \tilde{p}_2 \in [0, 1)$). This expression is obtained by expanding the MTG basis states using Eq. (28) and making use of the operator identity (see Appendix A):

$$\hat{t}^s(\mathbf{a}_1) = e^{i\frac{s(s-1)}{2}\mathbf{q}_\phi\cdot\mathbf{a}_1} e^{-is\mathbf{q}_\phi\cdot\mathbf{r}} \hat{T}^s(\mathbf{a}_1). \tag{42}$$

We hereby split the full single-electron Hamiltonian into the zero-field component $\hat{H}_0$ and the finite-field component $\hat{H}_{\mathbf{B}} = \hat{H} - \hat{H}_0$ and calculate each term separately.

#### 1. $\hat{H}_0$

For the zero-field Hamiltonian, its matrix elements can be straightforwardly studied as follows:

$$\begin{aligned} I_1 = & \sum_{s,s_0,\gamma} e^{i2\pi k_1 s} e^{i\frac{s(s-1)}{2}\mathbf{q}_\phi\cdot\mathbf{a}_1} \langle w_\alpha(0, \tilde{k}_2)|\hat{H}_0|w_\gamma(s_0, \tilde{k}_2)\rangle \\ & \times \langle w_\gamma(s_0, \tilde{k}_2)|e^{-is\mathbf{q}_\phi\cdot\mathbf{r}}|w_\beta(s, \tilde{p}_2)\rangle, \end{aligned} \tag{43}$$

where we have inserted the narrow-band projector $\sum_{s_0\gamma}|w_\gamma(s_0, \tilde{k}_2)\rangle\langle w_\gamma(s_0, \tilde{k}_2)|$. The second line can be calculated by writing down hWSs in the Bloch band basis using Eq. (23):

$$\begin{aligned} & \langle w_\alpha(0, \tilde{k}_2)|\hat{H}_0|w_\gamma(s_0, \tilde{k}_2)\rangle \\ &= \frac{1}{N_1}\sum_{\tilde{k}_1, n} e^{-i2\pi\tilde{k}_1 s_0}[U^\dagger_{\alpha,n}(\tilde{\mathbf{k}})\varepsilon_{n,\tilde{\mathbf{k}}}U_{n,\gamma}(\tilde{\mathbf{k}})], \end{aligned} \tag{44}$$

where in this section we redefine $\tilde{\mathbf{k}} = \tilde{k}_1\mathbf{g}_1 + \tilde{k}_2\mathbf{g}_2$ ($\tilde{k}_1, \tilde{k}_2 \in [0, 1)$). It leads to one-dimensional (1D) hopping between

hWSs at different localization centers with the same wave vector $\tilde{k}_2$. The last line in Eq. (43) can be calculated as

$$\langle w_\gamma(s_0,\tilde{k}_2)|e^{-is\mathbf{q}_\phi\cdot\mathbf{r}}|w_\beta(s,\tilde{p}_2)\rangle = \frac{1}{N_1}\sum_{\tilde{k}_1,\tilde{p}_1} e^{i2\pi\tilde{k}_1 s_0}e^{-i2\pi\tilde{p}_1 s} \times \sum_{n,m} U^\dagger_{\gamma,n}(\tilde{\mathbf{k}})\langle\psi_n(\tilde{\mathbf{k}})|e^{-is\mathbf{q}_\phi\cdot\mathbf{r}}|\psi_m(\tilde{\mathbf{p}})\rangle U_{m,\beta}(\tilde{\mathbf{p}}). \quad (45)$$

It represents scattering between Bloch eigenstates by wave vector $s\mathbf{q}_\phi$. Therefore, the matrix elements of the zero-field Hamiltonian in the MTG basis represent a hop along the $\mathbf{a}_1$ direction, followed by magnetic scattering by wave vector $s\mathbf{q}_\phi$. Note that if $\mathbf{a}_1\cdot\mathbf{a}_2\neq 0$, i.e., we have nonorthogonal unit cell vectors such as a triangular or honeycomb lattice, magnetic scattering hybridizes Bloch states with wave vectors $\tilde{\mathbf{k}}=\tilde{k}_1\mathbf{g}_1+\tilde{k}_2\mathbf{g}_2$ and $\tilde{\mathbf{p}}=\tilde{p}_1\mathbf{g}_1+\tilde{p}_2\mathbf{g}_2$ such that

$$\tilde{p}_1=\left[\tilde{k}_1+\frac{sp}{q}\frac{a_{1y}}{a_2}\right]_1,\ r_2=[r_1+sp]_q. \quad (46)$$

### 2. $\hat{H}_\mathbf{B}$

The finite-field term in the Landau gauge is given by $\hat{H}_\mathbf{B}(\mathbf{r})=\frac{\hbar x\hat{p}_y}{m_e\ell^2}+\frac{\hbar^2x^2}{2m_e\ell^4}$. It contains polynomials of the coordinates and grows when moving away from the axes' origin, where $x=0$. Below we work out the matrix elements for the term $\frac{\hbar x\hat{p}_y}{m_e\ell^2}$, and the second term can be calculated in an analogous fashion. Specifically,

$$I_2=\sum_s e^{i2\pi k_1 s}e^{i\frac{s(s-1)}{2}\mathbf{q}_\phi\cdot\mathbf{a}_1} \times\frac{\hbar^2}{m_e\ell^2}\langle w_\alpha(0,\tilde{k}_2)|\frac{x\hat{p}_y}{\hbar}e^{-is\mathbf{q}_\phi\cdot\mathbf{r}}|w_\beta(s,\tilde{p}_2)\rangle. \quad (47)$$

We first note that since the hWSs are exponentially suppressed away from their localization centers, for $s\gg 0$, the term is exponentially small regardless of the operator. Using the estimate $\langle x\rangle\sim a_{1x}$ and $\langle\hat{p}_y\rangle\sim 2\pi\hbar/a_2$, $I_2\sim\frac{\hbar^2}{m_e\ell^2}$, i.e., cyclotron frequency. At low fields such that $p/q\ll 1$, the finite-field term is smaller than the zero-field term by the ratio $p/q$. Therefore, unless there are further band flattening effects for the zero-field term (e.g., TBG at the magic angle), the finite-field term is negligible.

The second line of Eq. (47) can be calculated by expanding in the Bloch basis:

$$\frac{\hbar}{m_e\ell^2N_1}\sum_{\tilde{k}_1\tilde{p}_1}e^{-i2\pi\tilde{p}_1 s} \times\sum_{n,m}U^\dagger_{\alpha,n}(\tilde{\mathbf{k}})U_{m,\beta}(\tilde{\mathbf{p}})\langle\psi_n(\tilde{\mathbf{k}})|\frac{x\hat{p}_y}{\hbar}e^{-is\mathbf{q}_\phi\cdot\mathbf{r}}|\psi_m(\tilde{\mathbf{p}})\rangle, \quad (48)$$

where the second line can be explicitly calculated in the plane wave basis:

$$\langle\psi_n(\tilde{\mathbf{k}})|\frac{x\hat{p}_y}{\hbar}e^{-is\mathbf{q}_\phi\cdot\mathbf{r}}|\psi_m(\tilde{\mathbf{p}})\rangle = \sum_{\mathbf{g},\mathbf{g}'}u^*_{n\mathbf{g}}(\tilde{\mathbf{k}})u_{m\mathbf{g}'}(\tilde{\mathbf{p}})\frac{1}{\mathcal{A}}\int d^2\mathbf{r} \times e^{-i(\mathbf{g}+\tilde{\mathbf{k}})\cdot\mathbf{r}}[x(g_y+\tilde{k}_y)]e^{-is\mathbf{q}_\phi\cdot\mathbf{r}}e^{i(\mathbf{g}'+\tilde{\mathbf{p}})\cdot\mathbf{r}}. \quad (49)$$

Here we have expanded the periodic part of the Bloch states in a Fourier series: $u_{n\tilde{\mathbf{k}}}(\mathbf{r})=\sum_\mathbf{g}e^{i\mathbf{g}\cdot\mathbf{r}}u_{n\mathbf{g}}(\tilde{\mathbf{k}})$, and $\mathcal{A}=N_1N_2a_{1x}a_{2y}$ is the area of the system. It is important that the real space integral $\int d^2\mathbf{r}[\cdots]$ must be placed in a box to avoid revivals of the hWSs along the $\mathbf{e}_x$ direction at the boundary of a torus. In practice we choose the integration domain to be $x\in[-\frac{N_1a_{1x}}{2},-\frac{N_1a_{1x}}{2})$ (see Appendix B for details).

### E. Comparing Hofstadter spectra

In Fig. 4 we show a comparison of the Hofstadter spectra for the lowest-energy Bloch band with square [Figs. 4(a)–4(c)] and triangular [Figs. 4(d)–4(f)] lattice potentials, calculated using the exact LL approach and the approximate hWS approach. For the parameters used in the calculation, the hWSs are well localized within a unit cell (see Fig. 1), and there is good quantitative agreement of the Hofstadter spectra up to $\phi/\phi_0\approx 0.2$. At higher magnetic flux, the MTG states generated from hWSs have a larger spillover onto remote magnetic subbands and lead to an overall upward shift of the Hofstadter spectra when compared to LL calculations. Despite the quantitative differences in the Hofstadter spectra, the prominent magnetic subbands and the Chern numbers associated with gaps are correctly captured via the hWS method all the way to $\phi/\phi_0=1$, as indicated by the labels in Figs. 4(a), 4(b), 4(d), and 4(e).

### F. Harper equation

Equation (41) gives a general procedure for calculating the matrix elements of the single-electron Hamiltonian for a subset of Bloch bands isolated from the rest by making use of the hWSs at zero field and projecting onto representations of the MTG at finite field. Here we elaborate on the case of a square lattice potential and an isolated band with trivial topology. As mentioned, in this case the hWSs are just the 1D Fourier transforms of the Bloch eigenstates with a smooth gauge in the Brillouin zone, and the relation to 2D Wannier orbitals is described in Eq. (36). Below we show that the Harper equation of Hofstadter [42] is recovered as long as the magnetic length $\ell$ is much longer than the localization length $\xi$ of the Wannier orbitals. We express the left-hand side of Eq. (45) using 2D exponentially localized Wannier orbitals,

$$\langle w(s_0,\tilde{k}_2)|e^{-is\mathbf{q}_\phi\cdot\mathbf{r}}|w(s,\tilde{p}_2)\rangle = \frac{1}{N_2}\sum_{n_1,n_2}\left[\int d^2\mathbf{r}\phi^*_{\mathbf{R}_1}(\mathbf{r})\phi_{\mathbf{R}_2}(\mathbf{r})e^{-is\mathbf{q}_\phi\cdot(\mathbf{r}-\mathbf{R}_2)}\right] \times e^{-is\mathbf{q}_\phi\cdot\mathbf{R}_2}e^{-i2\pi\tilde{k}_2n_1}e^{i2\pi\tilde{p}_2n_2}, \quad (50)$$

where we define $\mathbf{R}_1=s_0\mathbf{a}_1+n_1\mathbf{a}_2$ and $\mathbf{R}_2=s\mathbf{a}_1+n_2\mathbf{a}_2$. Since Wannier orbitals are exponentially localized, $s_0$ and $s_1$ have to be close to each other. Making the assumption that the 1D hopping is short range, Eq. (44) forces $s_0$ to be near zero; therefore, $s$ is also close to zero. As a result, the factor $e^{-is\mathbf{q}_\phi\cdot(\mathbf{r}-\mathbf{R}_2)}$ slowly varies over the length scale $\sim\xi$, the spatial extent of the exponentially localized Wannier orbital, and can be Taylor expanded in the real space integration in the brackets. The integral can therefore be expanded in power

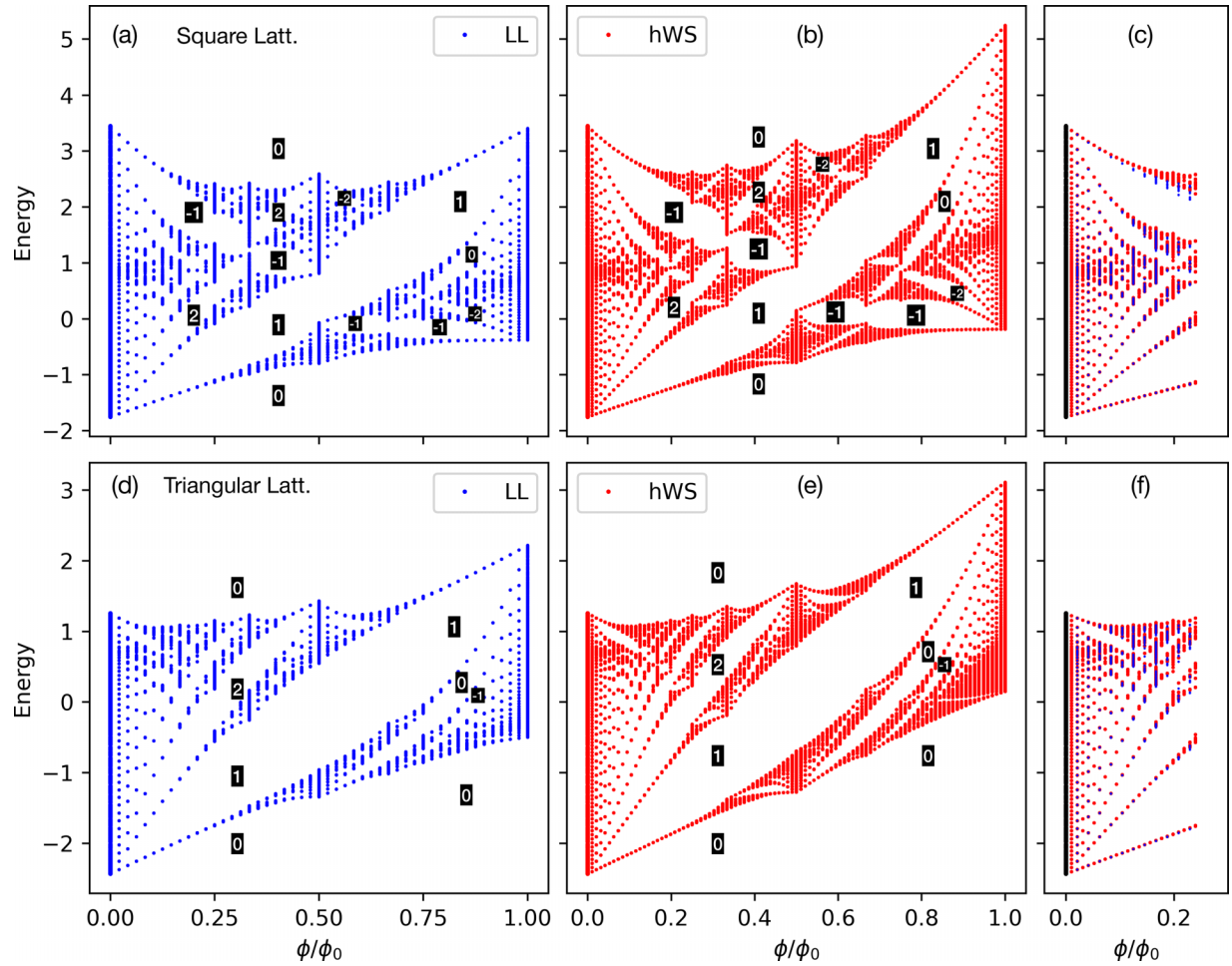


FIG. 4. Hofstadter spectra obtained using the exact LL approach (blue) and the hWS approach (red). Top panels are for the square lattice, and bottom panels are for the triangular lattice. Lattice potential strength $V_0 = 3$ is used. We set the energy scale as $\hbar^2/m_e a^2 = 1$. For the LL approach we studied the $p/q$ sequence for $q = 48$ and $p = 1, \ldots, 48$. For the hWS approach we studied the sequence $q = 96$ and $p = 1, \ldots, 96$. The numbers in the plots label the Chern number of the corresponding energy gaps.

series of $\xi/\ell$ as

$$\begin{aligned}&\int \mathrm{d}^2\mathbf{r}\phi^*_{\mathbf{R}_1}(\mathbf{r})\phi_{\mathbf{R}_2}(\mathbf{r})e^{-is\mathbf{q}_\phi\cdot(\mathbf{r}-\mathbf{R}_2)}\\ &\approx \int \mathrm{d}^2\mathbf{r}\phi^*_{\mathbf{R}_1}(\mathbf{r})\phi_{\mathbf{R}_2}(\mathbf{r})[1 - is\mathbf{q}_\phi\cdot(\mathbf{r}-\mathbf{R}_2)+\cdots]\\ &= \delta_{s_0,s}\delta_{n_1,n_2} + O(a_{1x}\xi/\ell^2).\end{aligned} \tag{51}$$

As a result, Eq. (50) becomes

$$\langle w(s_0,\tilde{k}_2)|e^{-is\mathbf{q}_\phi\cdot\mathbf{r}}|w(s,\tilde{p}_2)\rangle = \delta_{s_0,s}\delta_{[r_1+sp]_q,r_2} + O(a_{1x}\xi/\ell^2), \tag{52}$$

where in the last line we have substituted $\tilde{k}_2 = k_2 + r_1/q$ and $\tilde{p}_2 = k_2 + r_2/q$. Keeping the leading-order term in the above expression and combining it with Eq. (44), we get the following simplification for Eq. (43):

$$I_1 \approx \frac{1}{N_1}\sum_s e^{i2\pi k_1 s}\sum_{\tilde{k}_1} e^{-i2\pi\tilde{k}_1 s}\varepsilon_{\tilde{\mathbf{k}}}\delta_{[r_1+sp]_q,r_2}. \tag{53}$$

For well-localized Wannier states the dispersion can be approximated by nearest-neighbor hoppings, i.e., $\varepsilon_{\tilde{\mathbf{k}}} = 2E_0[\cos(2\pi\tilde{k}_1)+\cos(2\pi\tilde{k}_2)]$, and as a result

$$I_1 \approx E_0\left[2\cos(2\pi\tilde{k}_2)\delta_{r_1,r_2} + \sum_{s=\pm1} e^{i2\pi k_1 s}\delta_{[r_1+sp]_q,r_2}\right]. \tag{54}$$

We compare the above expression to the Harper equation obtained in Ref. [42]:

$$\begin{aligned}&g(m+1)+g(m-1)+2\cos\left(\frac{2\pi p}{q}m - 2\pi k_1\right)g(m)\\ &= \frac{E}{E_0}g(m),\end{aligned} \tag{55}$$

where we have replaced the notation $\nu$ used in Ref. [42] with $2\pi k_1$ and $\alpha$ with $p/q$. Performing Fourier series expansion of the wave function $g(m) = \sum_{k_2,r_2} e^{i2\pi(k_2+\frac{r_2}{q})m} g_{k_2,r_2}$ produces the eigenequation:

$$\begin{aligned}&E g_{k_2,r_1}\\ &= \sum_{r_2} E_0\left[2\cos(2\pi\tilde{k}_2)\delta_{r_1,r_2} + \sum_{s=\pm1} e^{i2\pi k_1 s}\delta_{[r_1+sp]_q,r_2}\right] g_{k_2,r_2}.\end{aligned} \tag{56}$$

The second line is precisely Eq. (54), explicitly recovering the Harper equation as a limiting case of the finite magnetic field problem when the magnetic length is much longer than the spatial extent of the Wannier orbital.

In Appendix E, we go beyond the nearest-neighbor hopping example discussed above and present a quantitative comparison of the Hofstadter spectra calculated using the Peierls substitution [39], the hWS approach, and the LL approach. As shown in Fig. 5, at lower magnetic flux ratios, both Peierls substitution and the hWS approach yield quantitatively accurate Hofstadter spectra. However, as magnetic flux is increased, the Peierls substitution approach becomes less accurate than the hWS approach at capturing the qualitative gap structures.

## IV. SUMMARY

Using the magnetic translation group projection method recently developed in Ref. [46] based on the $\mathbf{B} = 0$ hybrid Wannier states, we reexamined the Hofstadter physics of the $\mathbf{B} \neq 0$ magnetic subbands corresponding to a subset of energetically isolated and topologically trivial Bloch bands. Employing the continuum electron moving in 2D square and triangular lattice potentials as examples, we demonstrated that the method works well up to moderate strengths of magnetic flux per unit cell. Importantly, it naturally bridges the zero-field and finite-field Hilbert spaces. We also recovered the Harper equation [42] from the MTG states generated from hWSs and showed that its regime of validity is determined by the ratio of magnetic length to the size of exponentially localized Wannier orbitals.

Although here we applied this projection method only to the noninteracting Hamiltonians, the hWS procedure was shown to be useful in studying the interacting Hofstadter problem [46]. This is primarily due to two reasons: (1) At low magnetic fields, the procedure can faithfully construct the correct Hilbert space without having to increase the internal dimensions, unlike the conventional LL-based approach, where the upper LL index cutoff increases with decreasing field to achieve numerical convergence. (2) The plane wave nature of the hWSs makes the matrix representation of operators of the form $\mathcal{O}_{\mathbf{q}} e^{i\mathbf{q}\cdot\mathbf{r}}$ sparse. By comparison they are dense matrices in the LL wave function basis. This method can therefore efficiently address the effects of Coulomb interactions in a finite magnetic field in the presence of a periodic potential.

## ACKNOWLEDGMENTS

X.W. acknowledges financial support from the Gordon and Betty Moore Foundation's EPiQS Initiative Grant No. GBMF11070. O.V. was supported by NSF Grant No. DMR-1916958 and is partially funded by the Gordon and Betty Moore Foundation's EPiQS Initiative Grant No. GBMF11070, the National High Magnetic Field Laboratory through NSF Grant No. DMR-1157490, and the state of Florida.

## APPENDIX A: LANDAU GAUGE MAGNETIC TRANSLATION GROUP IDENTITIES

Here we derive an identity for $\hat{t}^s(\mathbf{a}_1)$, which is related to the zero-field discrete translation operator $\hat{T}(\mathbf{a}_1)$. Note that

$$\begin{aligned}
\hat{t}^s(\mathbf{a}_1) &= [e^{-i\mathbf{q}_\phi\cdot\mathbf{r}}\hat{T}(\mathbf{a}_1)]^{s-2}[e^{-i\mathbf{q}_\phi\cdot\mathbf{r}}\hat{T}(\mathbf{a}_1)][e^{-i\mathbf{q}_\phi\cdot\mathbf{r}}\hat{T}(\mathbf{a}_1)] \\
&= [e^{-i\mathbf{q}_\phi\cdot\mathbf{r}}\hat{T}(\mathbf{a}_1)]^{s-2} e^{i\mathbf{q}_\phi\cdot\mathbf{a}_1} e^{-i2\mathbf{q}_\phi\cdot\mathbf{r}}\hat{T}^2(\mathbf{a}_1) \\
&= [e^{-i\mathbf{q}_\phi\cdot\mathbf{r}}\hat{T}(\mathbf{a}_1)]^{s-3} e^{i(1+2)\mathbf{q}_\phi\cdot\mathbf{a}_1} e^{-i3\mathbf{q}_\phi\cdot\mathbf{r}}\hat{T}^3(\mathbf{a}_1) \\
&= e^{i[1+2+\cdots+(s-1)]\mathbf{q}_\phi\cdot\mathbf{a}_1} e^{-is\mathbf{q}_\phi\cdot\mathbf{r}}\hat{T}^s(\mathbf{a}_1) \\
&= e^{i\frac{s(s-1)}{2}\mathbf{q}_\phi\cdot\mathbf{a}_1} e^{-is\mathbf{q}_\phi\cdot\mathbf{r}}\hat{T}^s(\mathbf{a}_1). \qquad \text{(A1)}
\end{aligned}$$

We also show the MTG basis states $|\Psi_{n,r}(\mathbf{k})\rangle$, expressed using LL wave functions, form a complete set for $r = 0, \ldots, p-1$. It is sufficient to show that

$$|\Psi_{n,r+p}(\mathbf{k})\rangle = e^{i2\pi\left(k_1-(k_2+\frac{r}{q})\frac{a_{1y}}{a_2}\right)}|\Psi_{n,r}(\mathbf{k})\rangle, \qquad \text{(A2)}$$

namely, that states at $r+p$ and $r$ differ by a complex phase factor. Note that, by definition, in Eq. (10),

$$|\Psi_{n,r+p}(\mathbf{k})\rangle = \frac{1}{\sqrt{N}}\sum_{s=-\infty}^{\infty} e^{i2\pi k_1 s}\hat{t}^s(\mathbf{a}_1)\left|\psi_n\left(\frac{2\pi}{a_2}\left(k_2+\frac{r}{q}+\frac{p}{q}\right)\right)\right\rangle, \qquad \text{(A3)}$$

and the LL wave function is expressed in Eq. (1) as

$$\left|\psi_n\left(\tilde{k}_y+\frac{2\pi}{a_2}\frac{p}{q}\right)\right\rangle = e^{i\tilde{k}_y y} e^{i\frac{2\pi}{a_2}\frac{p}{q}y}\hat{T}\left(-\frac{2\pi}{a_2}\frac{p}{q}\ell^2\mathbf{e}_x\right)\hat{T}(-\tilde{k}_y\ell^2\mathbf{e}_x)|n\rangle. \qquad \text{(A4)}$$

Here we define $\tilde{k}_y \equiv \frac{2\pi}{a_2}(k_2+\frac{r}{q})$ for notational convenience. Note that

$$\frac{2\pi}{a_2}\frac{p}{q}\ell^2\mathbf{e}_x = \frac{1}{a_2}\frac{a_{1x}a_2}{\ell^2}\ell^2\mathbf{e}_x = a_{1x}\mathbf{e}_x \qquad \text{(A5)}$$

and that

$$\hat{T}(-a_{1x}\mathbf{e}_x)|n\rangle = \hat{T}(-\mathbf{a}_1)|n\rangle. \tag{A6}$$

Making use of the identity

$$\hat{t}(-\mathbf{a}_1) \equiv \hat{t}^\dagger(\mathbf{a}_1) = \hat{T}^\dagger(\mathbf{a}_1)e^{i\mathbf{q}_\phi\cdot\mathbf{r}} = e^{i\frac{2\pi}{a_2}\frac{p}{q}a_{1y}}e^{i\frac{2\pi}{a_2}\frac{p}{q}y}\hat{T}(-\mathbf{a}_1), \tag{A7}$$

we can rewrite Eq. (A4) as

$$\left|\psi_n\left(\tilde{k}_y + \frac{2\pi}{a_2}\frac{p}{q}\right)\right\rangle = e^{-i\frac{2\pi}{a_2}\frac{p}{q}a_{1y}}e^{i\tilde{k}_y y}\hat{t}(-\mathbf{a}_1)\hat{T}(-\tilde{k}_y\ell^2\mathbf{e}_x)|n\rangle = e^{-i\left(\tilde{k}_y+\frac{2\pi}{a_2}\frac{p}{q}\right)a_{1y}}\hat{t}(-\mathbf{a}_1)|\psi_n(\tilde{k}_y)\rangle. \tag{A8}$$

Here for the last equality we use $e^{i\tilde{k}_y y}\hat{t}(-\mathbf{a}_1) = e^{-i\tilde{k}_y a_{1y}}\hat{t}(-\mathbf{a}_1)e^{i\tilde{k}_y y}$. Substituting this back into Eq. (A3),

$$\begin{aligned}
|\Psi_{n,r+p}(\mathbf{k})\rangle &= e^{-i\frac{2\pi}{a_2}\left(k_2+\frac{r+p}{q}\right)a_{1y}}\frac{1}{\sqrt{N}}\sum_{s=-\infty}^{\infty}e^{i2\pi k_1 s}\hat{t}^s(\mathbf{a}_1)\hat{t}(-\mathbf{a}_1)\left|\psi_n\left(\frac{2\pi}{a_2}\left(k_2+\frac{r}{q}\right)\right)\right\rangle \\
&= e^{i2\pi\left(k_1-(k_2+\frac{r+p}{q})\frac{a_{1y}}{a_2}\right)}\frac{1}{\sqrt{N}}\sum_{s=-\infty}^{\infty}e^{i2\pi k_1(s-1)}\hat{t}^{s-1}(\mathbf{a}_1)\left|\psi_n\left(\frac{2\pi}{a_2}\left(k_2+\frac{r}{q}\right)\right)\right\rangle \\
&= e^{i2\pi\left(k_1-(k_2+\frac{r+p}{q})\frac{a_{1y}}{a_2}\right)}|\Psi_{n,r}(\mathbf{k})\rangle.
\end{aligned} \tag{A9}$$

## APPENDIX B: OVERLAP MATRIX

Here we show how to calculate the overlap matrix between MTG basis states generated from zero-field hybrid Wannier states, Eq. (32). Specifically, we define the overlap matrix $\Lambda_{\alpha r_1,\beta r_2}(k_1,k_2)$, where $k_1 \in [0,1)$, $k_2 \in [0,1/q)$, and $r_{1,2} = 0,\ldots,q-1$. It can be calculated by switching to the Bloch basis,

$$\begin{aligned}
\Lambda_{\alpha r_1,\beta r_2}(k_1,k_2) &= \sum_s e^{i2\pi k_1 s}e^{i\frac{s(s-1)}{2}\mathbf{q}_\phi\cdot\mathbf{a}_1}\left\langle w_\alpha\left(0,k_2+\frac{r_1}{q}\right)\middle|e^{-is\mathbf{q}_\phi\cdot\mathbf{r}}\middle|w_\beta\left(s,k_2+\frac{r_2}{q}\right)\right\rangle \\
&= \sum_s e^{i2\pi k_1 s}e^{i\frac{s(s-1)}{2}\mathbf{q}_\phi\cdot\mathbf{a}_1}\frac{1}{N_1}\sum_{\bar{k}_1\bar{p}_1}e^{-i2\pi\bar{p}_1 s}\left\langle\psi_\alpha\left(\bar{k}_1,k_2+\frac{r_1}{q}\right)\middle|e^{-is\mathbf{q}_\phi\cdot\mathbf{r}}\middle|\psi_\beta\left(\bar{p}_1,k_2+\frac{r_2}{q}\right)\right\rangle.
\end{aligned} \tag{B1}$$

In the second line we introduced the Bloch states $|\psi_\alpha(\mathbf{k})\rangle = \sum_n U_{n,\alpha}(\mathbf{k})|\psi_n(\mathbf{k})\rangle$, with the distinction that the subscript $\alpha$ labels Fourier transforms of the hWS and $n$ labels Bloch eigenstates. The second line is calculated in the plain wave basis by writing down $\langle\mathbf{r}|\psi_\alpha(\mathbf{k})\rangle = \sum_{\mathbf{g}} e^{i(\mathbf{k}+\mathbf{g})\cdot\mathbf{r}}u_{\mathbf{g}}(\alpha\mathbf{k})$. We arrive at the following expression:

$$\begin{aligned}
\Lambda_{\alpha r_1,\beta r_2}(k_1,k_2) = \sum_s e^{i2\pi k_1 s}e^{i\frac{s(s-1)}{2}\mathbf{q}_\phi\cdot\mathbf{a}_1}\frac{1}{N_1}\sum_{\bar{k}_1\bar{p}_1}\sum_{\mathbf{g},\mathbf{g}'}e^{-i2\pi\bar{p}_1 s}u^*_{\mathbf{g}}\left(\alpha,\bar{k}_1,k_2+\frac{r_1}{q}\right)u_{\mathbf{g}'}\left(\beta,\bar{p}_1,k_2+\frac{r_2}{q}\right) \\
\times\frac{1}{\mathcal{A}}\int \mathrm{d}^2\mathbf{r}e^{-i(\bar{\mathbf{k}}+\mathbf{g})\cdot\mathbf{r}}e^{-is\mathbf{q}_\phi\cdot\mathbf{r}}e^{i(\bar{\mathbf{p}}+\mathbf{g}')\cdot\mathbf{r}}.
\end{aligned} \tag{B2}$$

The second line gives the constraint $\bar{\mathbf{k}}+\mathbf{g}+s\mathbf{q}_\phi = \bar{\mathbf{p}}+\mathbf{g}'$, which is equivalent to

$$\bar{k}_1 + l_1 + \frac{sp}{q}\frac{a_{1y}}{a_2} = \bar{p}_1 + l_1',\ \frac{r_1}{q} + l_2 + \frac{sp}{q} = \frac{r_2}{q} + l_2'. \tag{B3}$$

## APPENDIX C: REAL SPACE INTEGRATION OF $x$ AND $x^2$

The single-electron Hamiltonian in a finite magnetic field contains terms such as $x\hat{p}_y$ and $x^2$; we hereby give analytical expressions for their real space integrations. In evaluating the matrix elements for the Hamiltonian, boundary terms do not matter, as the exponential localization of the hWSs guarantees that the main contributing terms to $\sum_s$ in Eq. (41) are restricted to the vicinity of $s=0$. We therefore choose the real space domain to contain $N_1$ and $N_2$ unit cells in the $\mathbf{a}_1$ and $\mathbf{a}_2$ directions and place the origin of the coordinate system at the center of the real space domain. Specifically, the integral is performed in the following manner:

$$\frac{1}{\mathcal{A}}\int \mathrm{d}^2\mathbf{r}[\cdots] = \frac{1}{N_1N_2}\frac{1}{a_{1x}a_2}\int_{-\frac{N_1}{2}a_{1x}}^{\frac{N_1}{2}a_{1x}}\mathrm{d}x\int_{\frac{a_{1y}}{a_{1x}}x-\frac{N_2}{2}a_2}^{\frac{a_{1y}}{a_{1x}}x+\frac{N_2}{2}a_2}\mathrm{d}y[\cdots]. \tag{C1}$$

As a result,

$$\frac{1}{\mathcal{A}}\int \mathrm{d}^2\mathbf{r}\left(\frac{x}{a_{1x}}\right)e^{i\mathbf{q}\cdot\mathbf{r}} = \delta_{q_y,0}(-i)\frac{\tilde{q}_x\cos\left(\frac{N_1}{2}\tilde{q}_x\right)-\frac{2}{N_1}\sin\left(\frac{N_1}{2}\tilde{q}_x\right)}{\tilde{q}_x^2}, \tag{C2}$$

and

$$\frac{1}{\mathcal{A}}\int \mathrm{d}^2\mathbf{r}\left(\frac{x}{a_{1x}}\right)^2 e^{i\mathbf{q}\cdot\mathbf{r}} = \delta_{q_y,0}\frac{4\tilde{q}_x\cos\left(\frac{N_1}{2}\tilde{q}_x\right)+\left(-\frac{8}{N_1}+N_1\tilde{q}_x^2\right)\sin\left(\frac{N_1}{2}\tilde{q}_x\right)}{2\tilde{q}_x^3}, \tag{C3}$$

where we define $\tilde{q}_x \equiv q_x a_{1x}$.

## APPENDIX D: OVERLAP BETWEEN MTG BASIS STATES GENERATED FROM LL APPROACH AND THE HWS APPROACH

To demonstrate the accuracy of the hWS approach we need to calculate its overlap with the exact wave functions, which can be obtained using the LL approach, as discussed for Eq. (34). Here we calculate the following expression:

$$\Lambda_{\Psi,W}(nr_1,\alpha r_2;\mathbf{k}) \equiv \langle\Psi_{n,r_1}(\mathbf{k})|W_{\alpha,r_2}(\mathbf{k})\rangle, \tag{D1}$$

where $n$ runs over LL indices, $\alpha$ runs over hWS indices, $r_1 = 0,\ldots,p-1$, and $r_2 = 0,\ldots,q-1$. Using the definitions (10) and (28), we have

$$\begin{aligned}\Lambda_{\Psi,W}(nr_1,\alpha r_2;\mathbf{k}) &= \sum_s e^{-i2\pi k_1 s}\left\langle\psi_n\left(k_2+\frac{r_1}{q}\right)\middle|\hat{t}_{\mathbf{a}_1}^{-s}\middle|w_\alpha\left(0,k_2+\frac{r_2}{q}\right)\right\rangle \\ &= \sum_s e^{-i2\pi k_1 s}e^{-i\frac{s(s-1)}{2}\mathbf{q}_\phi\cdot\mathbf{a}_1}e^{i2\pi(k_2+\frac{r_1}{q})\frac{a_{1y}}{a_2}s}\frac{1}{\sqrt{N_1}}\sum_{\bar{k}_1}\left\langle\psi_n\left(k_2+\frac{r_1}{q}-\frac{sp}{q}\right)\middle|\psi_\alpha\left(\bar{k}_1,k_2+\frac{r_2}{q}\right)\right\rangle.\end{aligned} \tag{D2}$$

We evaluate the overlap between a LL wave function with a Bloch wave function as follows:

$$\begin{aligned}&\left\langle\psi_n\left(k_2+\frac{r_1}{q}-\frac{sp}{q}\right)\middle|\psi_\alpha\left(\bar{k}_1,k_2+\frac{r_2}{q}\right)\right\rangle \\ &= \frac{1}{N_2a_2}\frac{1}{\sqrt{N_1a_{1x}\ell}}\sum_{\mathbf{g}}u_{\alpha\mathbf{g}}\int\mathrm{d}^2\mathbf{r}\phi_n\left[\frac{x}{\ell}+\frac{2\pi}{a_2}\left(k_2+\frac{r_1-sp}{q}\right)\ell\right]e^{-i\frac{2\pi}{a_2}(k_2+\frac{r_1-sp}{q})y}e^{i(\bar{\mathbf{k}}+\mathbf{g})\cdot\mathbf{r}} \\ &= \frac{1}{\sqrt{N_1a_{1x}\ell}}\sum_{\mathbf{g}}u_{\alpha\mathbf{g}}\delta_{\frac{r_1-sp}{q},\frac{r_2}{q}+l_2}\int\mathrm{d}x\phi_n\left[\frac{x}{\ell}+(\bar{k}_y+g_y)\ell\right]e^{i(\bar{k}_x+g_x)x} \\ &= \frac{1}{\sqrt{N_1a_{1x}\ell}}\sum_{\mathbf{g}}u_{\alpha\mathbf{g}}\delta_{\frac{r_1-sp}{q},\frac{r_2}{q}+l_2}e^{-i(\bar{k}_x+g_x)(\bar{k}_y+g_y)\ell^2}\int\mathrm{d}x\phi_n\left(\frac{x}{\ell}\right)e^{i(\bar{k}_x+g_x)x} \\ &= \frac{1}{\sqrt{N_1}}\sqrt{\frac{\ell}{a_{1x}}}\sum_{\mathbf{g}}u_{\alpha\mathbf{g}}\delta_{\frac{r_1-sp}{q},\frac{r_2}{q}+l_2}e^{-i(\bar{k}_x+g_x)(\bar{k}_y+g_y)\ell^2}\sqrt{2\pi}(i)^n\phi_n[(\bar{k}_x+g_x)\ell].\end{aligned} \tag{D3}$$

Here we define $\bar{\mathbf{k}} = \bar{k}_1\mathbf{g}_1 + (k_2+\frac{r_2}{q})\mathbf{g}_2 \equiv \bar{k}_x\mathbf{e}_x + \bar{k}_y\mathbf{e}_y$. In the second line we used the following definitions for the Bloch and LL wave functions:

$$\langle\mathbf{r}|\psi_\alpha(\mathbf{k})\rangle = \frac{1}{\sqrt{N_2a_2}}\frac{1}{\sqrt{N_1a_{1x}}}\sum_{\mathbf{g}}u_{\alpha\mathbf{g}}(\mathbf{k})e^{i(\mathbf{k}+\mathbf{g})\cdot\mathbf{r}}, \tag{D4}$$

$$\langle\mathbf{r}|\psi_n(k_2)\rangle = \frac{1}{\sqrt{N_2a_2}}\frac{1}{\sqrt{\ell}}\phi_n\left(\frac{x}{\ell}+\frac{2\pi}{a_2}k_2\ell\right)e^{i\frac{2\pi}{a_2}k_2y}, \tag{D5}$$

where

$$\phi_n\left(\frac{x}{\ell}\right) = \frac{1}{\pi^{1/4}\sqrt{2^n n!}}e^{-\frac{x^2}{2\ell^2}}H_n\left(\frac{x}{\ell}\right). \tag{D6}$$

## APPENDIX E: TIGHT-BINDING MODEL AND PEIERLS SUBSTITUTION

Here we present a calculation of the Hofstadter spectrum for a tight-binding model on a square lattice with one orbital per site and longer-range hoppings. The spectra are then compared to both the exact LL approach and the hybrid Wannier approach discussed in the main text.

The tight-binding Hamiltonian in zero magnetic field is given by

$$\hat{H}_{\mathrm{TB}} = \sum_{\mathbf{r}_1,\mathbf{r}_2} t(\mathbf{r}_1 - \mathbf{r}_2) c^\dagger_{\mathbf{r}_1} c_{\mathbf{r}_2} + \mathrm{H.c.}, \tag{E1}$$

where $\mathbf{r}_i = m_i\mathbf{a}_1 + n_i\mathbf{a}_2$ labels the positions of lattice sites, with $\{m_i, n_i\} \in \mathbb{Z}$. $t(\mathbf{r}_1 - \mathbf{r}_2)$ is the hopping amplitude between the two sites and depends only on the relative coordinate due to discrete translation symmetry $\hat{T}(\mathbf{a}_i)$, $i = 1, 2$. Its Fourier transform is the energy dispersion:

$$\varepsilon_{\mathbf{k}} = \sum_{\mathbf{r}_1-\mathbf{r}_2} t(\mathbf{r}_1 - \mathbf{r}_2) e^{-i\mathbf{k}\cdot(\mathbf{r}_1-\mathbf{r}_2)}, \tag{E2}$$

where $\mathbf{k} = k_1\mathbf{g}_1 + k_2\mathbf{g}_2$ is the wave vector in the Brillouin zone, with $k_1, k_2 \in [0, 1)$. $N_1$ and $N_2$ are the numbers of lattice sites along the $\mathbf{a}_1$ and $\mathbf{a}_2$ directions, respectively.

In a finite magnetic field, Peierls substitution [39] attaches a phase to the hopping amplitude:

$$t(\mathbf{r}_1 - \mathbf{r}_2) e^{-i\frac{e}{\hbar c}\int_{\mathbf{r}_1}^{\mathbf{r}_2} \mathrm{d}\mathbf{r}'\cdot\mathbf{A}(\mathbf{r}')} = t(\mathbf{r}_1 - \mathbf{r}_2) e^{-\frac{i}{2\ell^2}(r_{2y}-r_{1y})(r_{2x}+r_{1x})}, \tag{E3}$$

where, on the right-hand side, we use the Landau gauge $\mathbf{A} = Bx\mathbf{e}_y$.

At rational magnetic flux ratios $\phi/\phi_0 = p/q$, the phase factor in Eq. (E3) reduces to

$$-\frac{2\pi p}{q}(n_2 - n_1)\frac{m_1 + m_2}{2}, \ \mathbf{r}_{i=1,2} \equiv m_i\mathbf{a}_1 + n_i\mathbf{a}_2, \ m_i, n_i \in \mathbb{Z}. \tag{E4}$$

Therefore, the finite-field Hamiltonian is invariant under discrete translations $\hat{T}(q\mathbf{a}_1)$ and $\hat{T}(\mathbf{a}_2)$. As a result, the magnetic unit cell is enlarged along the $\mathbf{a}_1$ direction by $q$ times. We relabel the lattice sites as

$$\mathbf{r}_1 \to \mathbf{R}_1 + \vec{\tau}_\alpha, \ \mathbf{r}_2 \to \mathbf{R}_2 + \vec{\tau}_\beta, \tag{E5}$$

where $\mathbf{R}_{i=1,2} \equiv m_i(q\mathbf{a}_1) + n_i(\mathbf{a}_2)$ and $\vec{\tau}_\alpha \equiv \alpha\mathbf{a}_1$, with $\alpha = 0, \ldots, q-1$. The Peierls substituted hopping amplitude is therefore rewritten as

$$t(\mathbf{R}_1 + \vec{\tau}_\alpha - \mathbf{R}_2 - \vec{\tau}_\beta) e^{-i2\pi p(n_2-n_1)\left(\frac{m_1+m_2}{2}+\frac{\alpha+\beta}{2q}\right)}. \tag{E6}$$

We apply discrete Fourier transformation for the fermion annihilation operator:

$$c_{\mathbf{R}_1+\vec{\tau}_\alpha} = \frac{1}{\sqrt{N_1N_2/q}} \sum_{k_1\in[0,1/q)} \sum_{k_2\in[0,1)} c_{\alpha,k_1,k_2} e^{i2\pi k_1(qm_1+\alpha)} e^{i2\pi k_2 n_1}. \tag{E7}$$

It is straightforward to show that the finite-field Hamiltonian is diagonal with respect to quantum numbers $\{k_1, k_2\}$, and

$$\begin{aligned}\hat{H}_{\mathrm{TB}}(\mathbf{B}) = {} & \frac{q}{N_1N_2} \sum_{\alpha,\beta} \sum_{k_1,k_2} c^\dagger_{\alpha,k_1,k_2} c_{\beta,k_1,k_2} \frac{1}{N_1N_2} \sum_{p_1,p_2} \varepsilon_{p_1,p_2} \sum_{m_1,n_1,m_2,n_2} e^{i2\pi p_2(n_1-n_2)} e^{i2\pi p_1[(m_1-m_2)q+(\alpha-\beta)]} \\ & \times e^{-i2\pi p(n_2-n_1)\left(\frac{m_1+m_2}{2}+\frac{\alpha+\beta}{2q}\right)} e^{-i2\pi k_2(n_1-n_2)} e^{-i2\pi k_1[(m_1-m_2)q+(\alpha-\beta)]}.\end{aligned} \tag{E8}$$

Here $\mathbf{p} = p_1\mathbf{g}_1 + p_2\mathbf{g}_2$ is defined in the zero-field Brillouin zone with $p_1, p_2 \in [0, 1) \times [0, 1)$. We define the center of mass and relative coordinates as

$$M = \frac{m_1 + m_2}{2}, \ m = m_1 - m_2, \ N = \frac{n_1 + n_2}{2}, \ n = n_1 - n_2. \tag{E9}$$

Summing over center of mass position $Mq\mathbf{a}_1 + N\mathbf{a}_2$ trivially leads to

$$\hat{H}_{\mathrm{TB}}(\mathbf{B}) = \frac{1}{N_1N_2} \sum_{\alpha,\beta} \sum_{k_1,k_2} c^\dagger_{\alpha,k_1,k_2} c_{\beta,k_1,k_2} \sum_{p_1,p_2} \varepsilon_{p_1,p_2} \sum_{m,n} e^{i2\pi(p_2-k_2-\frac{p(\alpha+\beta)}{2q})n} e^{i2\pi(p_1-k_1)[mq+(\alpha-\beta)]}. \tag{E10}$$

Summing over $n$ and $m$ leads to

$$\hat{H}_{\mathrm{TB}}(\mathbf{B}) \equiv \sum_{\alpha,\beta} \sum_{k_1,k_2} c^\dagger_{\alpha,k_1,k_2} \hat{T}_{\alpha,\beta}(k_1, k_2) c_{\beta,k_1,k_2}, \tag{E11}$$

$$\hat{T}_{\alpha,\beta}(k_1, k_2) \equiv \frac{1}{q} \sum_{r_1,p_2} \varepsilon_{k_1+\frac{r_1}{q},p_2} e^{i2\pi\frac{r_1}{q}(\alpha-\beta)} \delta_{p_2,[k_2+\frac{p(\alpha+\beta)}{2q}]_1}. \tag{E12}$$

In Eq. (E12) we define $p_1 = [p_1]_{1/q} + \frac{r_1}{q}$, where $r_1 = 0, \ldots, q$, and $k_1 = [p_1]_{1/q}$. At any given wave vector $\mathbf{k} \equiv k_1\mathbf{g}_1 + k_2\mathbf{g}_2$, $\hat{T}_{\alpha,\beta}(k_1, k_2)$ is a $q \times q$ matrix. Diagonalizing $\hat{T}_{\alpha,\beta}(k_1, k_2)$ gives the $q$ Hofstadter subbands for a given flux ratio $\phi/\phi_0 = p/q$.

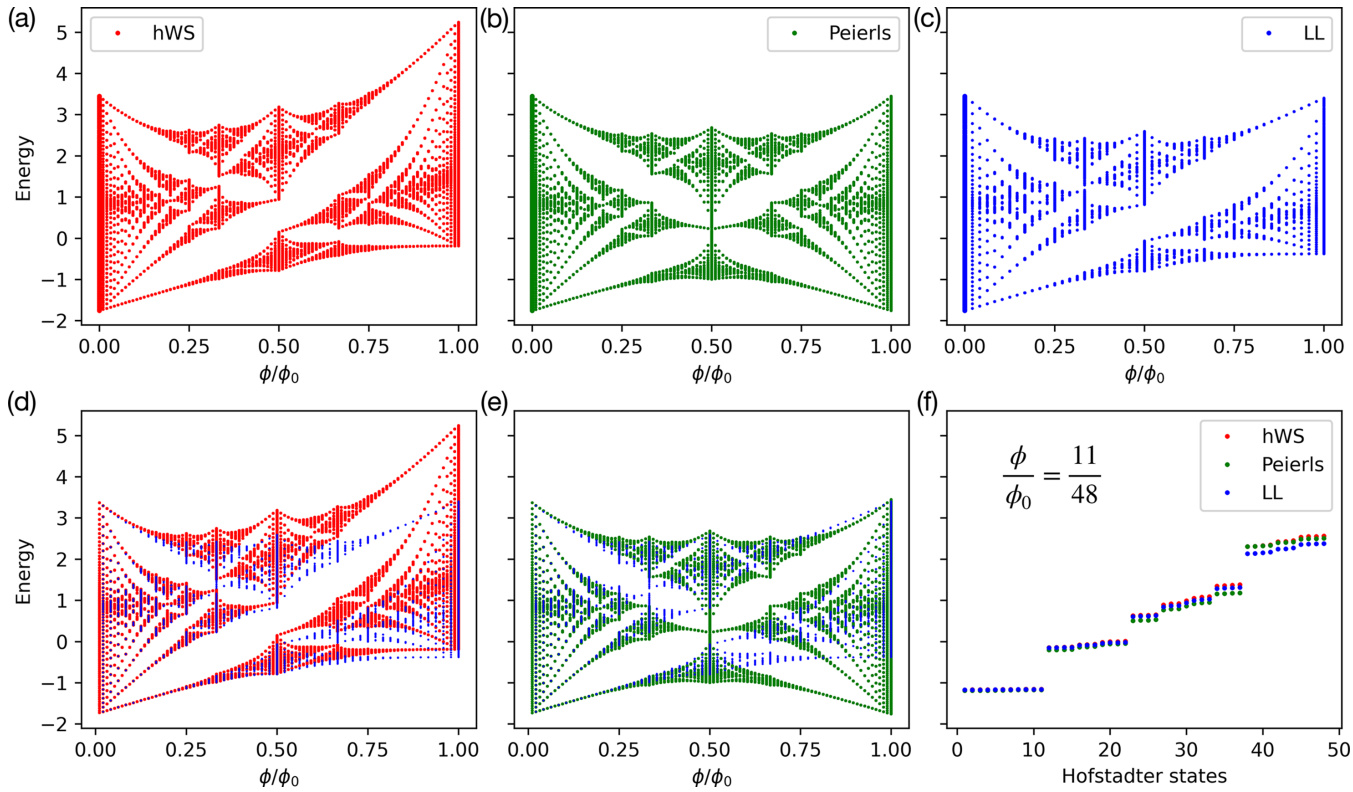


FIG. 5. Hofstadter spectrum for the square lattice potential used in Figs. 4(a)–4(c) in the main text, calculated using (a) the hybrid Wannier, (b) Peierls substitution, and (c) Landau level methods. (d) and (e) show more detailed overlay comparisons. (f) shows a comparison of the spectra calculated at wave vector $k_1 = k_2 = 0$ at magnetic flux ratio $\phi/\phi_0 = 11/48$.

In Fig. 5 we compare the Hofstadter spectra computed using the above Peierls substitution method (green) to the Landau level method (blue) and the hybrid Wannier method (red). The Peierls substitution method is in reasonably good agreement with the two other approaches at lower magnetic flux ratios [Fig. 5(f)]. However, at higher fluxes, the method leads to qualitatively different spectra. For example, at $\phi/\phi_0 = 1/2$, the Peierls substitution shows a gapless spectrum at half filling, instead of gapped spectra, as shown by both the Landau level and hybrid Wannier methods. Moreover, the Peierls substitution shows a periodic spectrum when magnetic flux is increased by the unit flux quantum due to the omission of the energetic effects of magnetic fields, i.e., $\hat{H}_{\mathbf{B}}$ in Sec. III D 2.


[1] Y. Cao, V. Fatemi, A. Demir, S. Fang, S. L. Tomarken, J. Y. Luo, J. D. Sanchez-Yamagishi, K. Watanabe, T. Taniguchi, E. Kaxiras, R. C. Ashoori, and P. Jarillo-Herrero, Nature (London) **556**, 80 (2018).

[2] Y. Cao, V. Fatemi, S. Fang, K. Watanabe, T. Taniguchi, E. Kaxiras, and P. Jarillo-Herrero, Nature (London) **556**, 43 (2018).

[3] Y. Cao, D. Rodan-Legrain, O. Rubies-Bigorda, J. M. Park, K. Watanabe, T. Taniguchi, and P. Jarillo-Herrero, Nature (London) **583**, 215 (2020).

[4] Y. Tang, L. Li, T. Li, Y. Xu, S. Liu, K. Barmak, K. Watanabe, T. Taniguchi, A. H. MacDonald, J. Shan, and K. F. Mak, Nature (London) **579**, 353 (2020).

[5] X. Liu, Z. Hao, E. Khalaf, J. Y. Lee, Y. Ronen, H. Yoo, D. Haei Najafabadi, K. Watanabe, T. Taniguchi, A. Vishwanath, and P. Kim, Nature (London) **583**, 221 (2020).

[6] L. Wang, E.-M. Shih, A. Ghiotto, L. Xian, D. A. Rhodes, C. Tan, M. Claassen, D. M. Kennes, Y. Bai, B. Kim, K. Watanabe, T. Taniguchi, X. Zhu, J. Hone, A. Rubio, A. N. Pasupathy, and C. R. Dean, Nat. Mater. **19**, 861 (2020).

[7] E. C. Regan, D. Wang, C. Jin, M. I. Bakti Utama, B. Gao, X. Wei, S. Zhao, W. Zhao, Z. Zhang, K. Yumigeta, M. Blei, J. D. Carlström, K. Watanabe, T. Taniguchi, S. Tongay, M. Crommie, A. Zettl, and F. Wang, Nature (London) **579**, 359 (2020).

[8] J. M. Park, Y. Cao, K. Watanabe, T. Taniguchi, and P. Jarillo-Herrero, Nature (London) **590**, 249 (2021).

[9] Z. Hao, A. M. Zimmerman, P. Ledwith, E. Khalaf, D. H. Najafabadi, K. Watanabe, T. Taniguchi, A. Vishwanath, and P. Kim, Science **371**, 1133 (2021).

[10] C. R. Kometter, J. Yu, T. Devakul, A. P. Reddy, Y. Zhang, B. A. Foutty, K. Watanabe, T. Taniguchi, L. Fu, and B. E. Feldman, arXiv:2212.05068.

[11] N. F. Q. Yuan and L. Fu, Phys. Rev. B **98**, 045103 (2018).
[12] M. Koshino, N. F. Q. Yuan, T. Koretsune, M. Ochi, K. Kuroki, and L. Fu, Phys. Rev. X **8**, 031087 (2018).
[13] J. Kang and O. Vafek, Phys. Rev. X **8**, 031088 (2018).
[14] H. C. Po, L. Zou, A. Vishwanath, and T. Senthil, Phys. Rev. X **8**, 031089 (2018).
[15] J. Kang and O. Vafek, Phys. Rev. Lett. **122**, 246401 (2019).
[16] B. A. Bernevig, Z.-D. Song, N. Regnault, and B. Lian, Phys. Rev. B **103**, 205411 (2021).
[17] Z.-D. Song, B. Lian, N. Regnault, and B. A. Bernevig, Phys. Rev. B **103**, 205412 (2021).
[18] B. A. Bernevig, Z.-D. Song, N. Regnault, and B. Lian, Phys. Rev. B **103**, 205413 (2021).
[19] B. Lian, Z.-D. Song, N. Regnault, D. K. Efetov, A. Yazdani, and B. A. Bernevig, Phys. Rev. B **103**, 205414 (2021).
[20] B. A. Bernevig, B. Lian, A. Cowsik, F. Xie, N. Regnault, and Z.-D. Song, Phys. Rev. B **103**, 205415 (2021).
[21] L. Balents, C. R. Dean, D. K. Efetov, and A. F. Young, Nat. Phys. **16**, 725 (2020).
[22] Z.-D. Song and B. A. Bernevig, Phys. Rev. Lett. **129**, 047601 (2022).
[23] C. R. Dean, L. Wang, P. Maher, C. Forsythe, F. Ghahari, Y. Gao, J. Katoch, M. Ishigami, P. Moon, M. Koshino, T. Taniguchi, K. Watanabe, K. L. Shepard, J. Hone, and P. Kim, Nature (London) **497**, 598 (2013).
[24] X. Lu, P. Stepanov, W. Yang, M. Xie, M. A. Aamir, I. Das, C. Urgell, K. Watanabe, T. Taniguchi, G. Zhang, A. Bachtold, A. H. MacDonald, and D. K. Efetov, Nature (London) **574**, 653 (2019).
[25] M. Yankowitz, S. Chen, H. Polshyn, Y. Zhang, K. Watanabe, T. Taniguchi, D. Graf, A. F. Young, and C. R. Dean, Science **363**, 1059 (2019).
[26] A. L. Sharpe, E. J. Fox, A. W. Barnard, J. Finney, K. Watanabe, T. Taniguchi, M. A. Kastner, and D. Goldhaber-Gordon, Science **365**, 605 (2019).
[27] K. P. Nuckolls, M. Oh, D. Wong, B. Lian, K. Watanabe, T. Taniguchi, B. A. Bernevig, and A. Yazdani, Nature (London) **588**, 610 (2020).
[28] A. T. Pierce, Y. Xie, J. M. Park, E. Khalaf, S. H. Lee, Y. Cao, D. E. Parker, P. R. Forrester, S. Chen, K. Watanabe, T. Taniguchi, A. Vishwanath, P. Jarillo-Herrero, and A. Yacoby, Nat. Phys. **17**, 1210 (2021).
[29] Y. Saito, J. Ge, L. Rademaker, K. Watanabe, T. Taniguchi, D. A. Abanin, and A. F. Young, Nat. Phys. **17**, 478 (2021).
[30] S. Wu, Z. Zhang, K. Watanabe, T. Taniguchi, and E. Y. Andrei, Nat. Mater. **20**, 488 (2021).
[31] J. Finney, A. L. Sharpe, E. J. Fox, C. L. Hsueh, D. E. Parker, M. Yankowitz, S. Chen, K. Watanabe, T. Taniguchi, C. R. Dean, A. Vishwanath, M. A. Kastner, and D. Goldhaber-Gordon, Proc. Natl. Acad. Sci. USA **119**, e2118482119 (2022).
[32] J. Yu, B. A. Foutty, Z. Han, M. E. Barber, Y. Schattner, K. Watanabe, T. Taniguchi, P. Phillips, Z.-X. Shen, S. A. Kivelson, and B. E. Feldman, Nat. Phys. **18**, 825 (2022).
[33] K. Hejazi, C. Liu, and L. Balents, Phys. Rev. B **100**, 035115 (2019).
[34] Y.-H. Zhang, H. C. Po, and T. Senthil, Phys. Rev. B **100**, 125104 (2019).
[35] B. Lian, F. Xie, and B. A. Bernevig, Phys. Rev. B **103**, L161405 (2021).
[36] J. Herzog-Arbeitman, A. Chew, D. K. Efetov, and B. A. Bernevig, Phys. Rev. Lett. **129**, 076401 (2022).
[37] D. Parker, P. Ledwith, E. Khalaf, T. Soejima, J. Hauschild, Y. Xie, A. Pierce, M. P. Zaletel, A. Yacoby, and A. Vishwanath, arXiv:2112.13837.
[38] J. Herzog-Arbeitman, A. Chew, and B. A. Bernevig, Phys. Rev. B **106**, 085140 (2022).
[39] R. Peierls, Z. Phys. **80**, 763 (1933).
[40] J. M. Luttinger, Phys. Rev. **84**, 814 (1951).
[41] P. G. Harper, Proc. Phys. Soc., Sect. A **68**, 874 (1955).
[42] D. R. Hofstadter, Phys. Rev. B **14**, 2239 (1976).
[43] A. A. Soluyanov and D. Vanderbilt, Phys. Rev. B **83**, 035108 (2011).
[44] H. C. Po, H. Watanabe, and A. Vishwanath, Phys. Rev. Lett. **121**, 126402 (2018).
[45] X. Wang and O. Vafek, Phys. Rev. B **102**, 075142 (2020).
[46] X. Wang and O. Vafek, Phys. Rev. B **106**, L121111 (2022).
[47] C. Sgiarovello, M. Peressi, and R. Resta, Phys. Rev. B **64**, 115202 (2001).
[48] R. Yu, X. L. Qi, A. Bernevig, Z. Fang, and X. Dai, Phys. Rev. B **84**, 075119 (2011).
[49] N. Marzari, A. A. Mostofi, J. R. Yates, I. Souza, and D. Vanderbilt, Rev. Mod. Phys. **84**, 1419 (2012).
[50] J. Kang and O. Vafek, Phys. Rev. B **102**, 035161 (2020).